bioRxiv preprint doi: https://doi.org/10.1101/2025.11.19.689269; this version posted November 19, 2025. The copyright holder for this preprint (which was not certified by peer review) is the author/funder, who has granted bioRxiv a license to display the preprint in perpetuity. It is made available under aCC-BY 4.0 International license.

Cardiac Hemorrhage Precedes Hypertension-induced Fibrosis in Plasminogen Activator Inhibitor-1 Deficient Mice

Alex C. Pettey,[1,2] Sohei Ito,[2] Michael K. Franklin,[2] Deborah A. Howatt,[2] Jessica J. Moorleghen,[2] Bryana M. Levitan,[1] David B. Graf,[2] Valerie Z. Guzmán,[2] Nancy Zhang,[2] Hisashi Sawada,[1-3] Jeffrey E. Saffitz,[4] Hong S. Lu,[1-3] Alan Daugherty[1-3]

[1] Department of Physiology,
[2] Saha Cardiovascular Research Center
[3] Saha Aortic Center
University of Kentucky, Lexington, KY

[4] Department of Pathology, Beth Israel Deaconess Medical Center,
Harvard Medical School, Boston, MA

Corresponding authors:
Alan Daugherty
Saha CVRC, BBSRB, Room 243
University of Kentucky
741 S Limestone
Lexington KY 40356-0509
e-mail – alan.daugherty@uky.edu

Hong S. Lu
Saha CVRC, BBSRB, Room 249
University of Kentucky
741 S Limestone
Lexington KY 40356-0509
e-mail – Hong.Lu@uky.edu

bioRxiv preprint doi: https://doi.org/10.1101/2025.11.19.689269; this version posted November 19, 2025. The copyright holder for this preprint (which was not certified by peer review) is the author/funder, who has granted bioRxiv a license to display the preprint in perpetuity. It is made available under aCC-BY 4.0 International license.

ABSTRACT

Aims:

Plasminogen activator inhibitor-1 (PAI-1) regulates plasmin-mediated proteolysis, thereby influencing vascular stability and tissue remodeling. Angiotensin II (AngII) induces an increase of PAI-1 during the development of ascending thoracic aortic aneurysm (ATAA). The purpose of this study was to determine whether deletion of PAI-1 influenced the development of ATAA.

Methods and results:

AngII was infused for 4 weeks in whole-body PAI-1 deficient (PAI-1-/-) mice and their wild-type littermates (PAI-1+/+) to examine the role of PAI-1 in ATAA. PAI-1 deficiency did not alter AngII-induced aortopathy but revealed a striking cardiac phenotype characterized by replacement fibrosis predominantly within the epicardium and posterior septum. Ferric iron, indicative of prior hemorrhage, was coincident with fibrosis. Similar phenotypes were observed in PAI-1-/- mice infused with norepinephrine for 4 weeks. To define the pathological events preceding cardiac fibrosis, either AngII or norepinephrine was infused for 1 week in PAI-1+/+ or -/- mice. Both infusions induced extensive epicardial hemorrhage and posterior septal fibrosis in PAI-1-/- mice. To explore the initiation of hemorrhage and fibrosis, mice were infused with AngII for approximately 1 day, resulting in diffuse hemorrhage and cardiomyocyte loss localized to the posterior septum of PAI-1-/- mice.

Conclusions:

These findings support that, under hemodynamic stress, PAI-1 deficiency promotes early cardiac hemorrhage and cardiomyocyte loss, implicating plasmin-mediated proteolysis as an initiator of cardiac injury and fibrosis.

TRANSLATIONAL PERSPECTIVE

Cardiac fibrosis has been reported in a human population with PAI-1 deficiency and currently lacks targeted therapy. Our findings demonstrate that in animal models, PAI-1 deficiency confers susceptibility to cardiac injury in response to hemodynamic stress, which may accelerate fibrotic remodeling. These observations suggest that interventions aimed at controlling hypertension, promoting endothelial integrity, or regulating plasmin activation could reduce fibrotic remodeling in this population.

bioRxiv preprint doi: https://doi.org/10.1101/2025.11.19.689269; this version posted November 19, 2025. The copyright holder for this preprint (which was not certified by peer review) is the author/funder, who has granted bioRxiv a license to display the preprint in perpetuity. It is made available under aCC-BY 4.0 International license.

INTRODUCTION

Cardiovascular diseases (CVDs) are a leading cause of death globally and represent a major healthcare burden (1). Despite therapeutic advances, many forms of CVD lack effective treatments, particularly aortic aneurysms and cardiomyopathies (2, 3). This need has motivated continued investigation into the molecular mechanisms that contribute to cardiovascular pathologies. Plasminogen activator inhibitor-1 (PAI-1), a serine protease inhibitor, has been implicated in several CVDs and has received considerable attention as a potential therapeutic target (4, 5). In experimental models, genetic deficiency of PAI-1 in mice reduces fibrosis in most organs (6). In contrast, PAI-1 deficient mice develop spontaneous cardiac fibrosis with aging, and show exacerbated fibrosis in response to angiotensin II (AngII) infusion, either alone or in combination with aldosterone (7-13). PAI-1 has also been reported to limit the development of abdominal aortic aneurysms (AAAs) (14-17). Overall, observations in animal models suggest that PAI-1 exerts context-dependent protective or adverse effects in CVD.

PAI-1 is the primary inhibitor of tissue-type (tPA) and urokinase-type (uPA) plasminogen activators and thereby limits plasminogen activation (4, 18). Through regulation of plasmin-mediated proteolysis, PAI-1 contributes to fibrin stability and influences extracellular matrix (ECM) turnover by restricting direct degradation of ECM or modulating activation of matrix metalloproteinases (MMPs) (18). These functions place PAI-1 at the interface of vascular integrity and tissue remodeling. Previous studies reported that pharmacological inhibition or genetic deficiency of PAI-1 attenuates AngII-induced aortic remodeling in mice (8, 13). Consistent with this finding, our recent study demonstrated that PAI-1 protein was increased markedly in the ascending aortas of AngII-infused mice and was abundant in human ascending thoracic aortic aneurysm (ATAA), implicating a potentially pathological role of PAI-1 in ATAA. While PAI-1 has been shown to protect against AAA in animal models (14-17), its role in ATAA, a disease process distinct from AAA, has not yet been reported.

To determine the role of PAI-1 in ATAA, whole-body PAI-1 deficient mice (PAI-1-/-) and their wild-type littermates (PAI-1+/+) were infused with AngII for 4 weeks. PAI-1 deficiency did not alter AngII-induced ATAA. Consistent with previous studies (8, 11-13), pronounced cardiac fibrosis was observed in AngII-infused PAI-1-/- mice. This phenotype was evident in both male and female mice. Prior reports have suggested that PAI-1 may protect against microvascular injury in the heart (9, 12), but the link between vascular integrity and cardiac fibrosis has not been defined. Moreover, the sequence of pathological events by which PAI-1 deficiency promotes cardiac fibrosis remains uncertain. Therefore, temporal and spatial characterizations were determined of cardiac pathologies exacerbated by PAI-1 deficiency. Further, norepinephrine (NE) was infused at a pressor rate to dissect the roles of hypertension versus other effects of AngII on development of cardiac pathologies in PAI-1-/- mice.

bioRxiv preprint doi: https://doi.org/10.1101/2025.11.19.689269; this version posted November 19, 2025. The copyright holder for this preprint (which was not certified by peer review) is the author/funder, who has granted bioRxiv a license to display the preprint in perpetuity. It is made available under aCC-BY 4.0 International license.

METHODS

Mice

PAI-1+/- (B6.129S2-*Serpine1*^{tm1Mlg}/J, Strain #002507) mice were purchased from The Jackson Laboratory. All study mice (littermates) were generated from male and female PAI-1+/- breeders. Mice were maintained on a 14-hour light/10-hour dark cycle at a controlled temperature of 20-23 °C and had free access to water and a standard laboratory diet (#2918, Inotiv). Inclusion and exclusion criteria for study mice were described in the Supplemental Materials following ARRIVE Guidelines Checklist (19).

Subcutaneous infusion using an osmotic mini pump

Mice (8 to 14-weeks of age) were infused in separate studies with saline, AngII, or NE through subcutaneously implanted osmotic mini pumps. AngII (1,000 ng/kg/min, #H-1705, Bachem) was dissolved in saline. NE (5.6 mg/kg/day, #A9512, Millipore Sigma) was dissolved in L-ascorbic acid (0.2% w/v in saline, #A65-21, Fisher Scientific) and protected from light. For 1 day or 1 week of infusion, osmotic mini pumps (Alzet model 1007D or 2001) were primed overnight at 37 °C in saline to initiate reagent release before pump implantation. For 4 weeks of infusion, osmotic mini pumps (Alzet model 1004) were primed overnight at 37 °C in saline to initiate infusion approximately 1 day after pump implantation, and surgical staples used to close incision sites were removed 7 days after surgery. Postoperative pain was alleviated by application of topical lidocaine cream (4% wt/wt, #59-930, HealthWise).

Ultrasound measurements

Ultrasonography was performed by an investigator blinded to the mouse identity. Ultrasound images were captured using a Vevo 3100 system equipped with a MX550D (25–55 MHz) linear transducer (VisualSonics, Fujifilm). Mice were anesthetized using inhaled isoflurane (2-3% vol/vol) and maintained at a heart rate of >400 beats per minute during image capture to reduce anesthesia exposure and maintain consistent heart rates between animals (SomnoFlo, Kent Scientific). The order in which mice were subject to ultrasound was not pre-selected. Image capture and data analysis were performed with animal genotype, infusion, and sex blinded.

Aortic imaging was performed using our standardized protocols (20). Briefly, images of the ascending aorta were captured using the right parasternal view and standardized according to two anatomical landmarks: the innominate artery branch point and the aortic valve. Aortic lumen was defined as the edge-to-edge distance of the ascending aortic wall between the sinotubular junction and the innominate artery. The largest luminal diameters of ascending aortas were measured in end-diastole over three cardiac cycles and averaged.

The heart was visualized from the modified parasternal long-axis and short-axis views. The left ventricular dimensions and calculated left ventricular ejection fraction were measured from the short-axis M-mode view (21). Left ventricular systolic strain

bioRxiv preprint doi: https://doi.org/10.1101/2025.11.19.689269; this version posted November 19, 2025. The copyright holder for this preprint (which was not certified by peer review) is the author/funder, who has granted bioRxiv a license to display the preprint in perpetuity. It is made available under aCC-BY 4.0 International license.

was derived from Vevo LAB (v5.8.2, Visual Sonics) utilizing speckle tracking of the modified parasternal long-axis and short-axis images. Each mouse consisted of three technical replicates that were averaged.

Quantification of aortic diameters using *in situ* images

Mice surviving 4 weeks of AngII infusion were euthanized by a cocktail of ketamine and xylazine (90 mg/kg #11695–6840-1, 10 mg/kg #11695–4024-1, respectively; Covetrus). The right atrial appendage was excised, and saline (~10 ml) was perfused via the left ventricle. Periaortic tissues were dissected carefully out, and a black plastic sheet was inserted underneath the aorta to improve image contrast (22, 23). A millimeter ruler was placed next to the aorta for calibration of measurements. *In situ* aortic images were captured with a Nikon SMZ25 stereoscope (Nikon). Aortic images were analyzed using NIS-Elements AR software (Version 5.11, Nikon). To measure aortic diameters, a measurement line was drawn perpendicularly to the aortic axis at the most dilated area of the ascending aorta. Measurements were verified by an individual who was blinded to the study groups.

Histology and immunostaining

Samples were randomly selected for histology when no gross pathology was observed, or to represent the full range of observed gross pathology when present. For histological analyses, tissues were harvested from surviving mice, immersed in neutral-buffered formalin (10% w/v), incubated in ethanol (70% v/v), and subsequently embedded in paraffin. Paraffin-embedded sections (5 µm) were deparaffinized using limonene (#183164, Millipore-Sigma). Masson's trichrome (#ab150686, abcam) staining was performed according to the manufacturer's protocol. For Verhoeff elastin staining, sections were stained with Verhoeff iron hematoxylin (hematoxylin 2.8% w/v, #3803815, Surgipath; ferric chloride 2.2% w/v, #3120-32, Bicca; iodine 0.4% w/v, #041955.22, Thermo Scientific; and potassium iodide 0.9% w/v, #0512, VWR; in 56% v/v ethanol) for 20 minutes and destained in 2% ferric chloride for 1-2 minutes. For Prussian blue staining, sections were stained with 1% w/v potassium ferrocyanide (#424135000, Thermo Scientific) in hydrochloric acid (0.37% v/v, #258148, Millipore Sigma) for 30 minutes and destained in neutral red (0.33% w/v, #N2889, Millipore Sigma) for 5 minutes.

Immunostaining was performed using blocking reagents, primary, and secondary antibodies listed in the Supplementary Materials Major Resources Tables. Deparaffinized sections were incubated with H_2O_2 (1% v/v, #H325, Fisher Scientific; in methanol) for 2 minutes at 40 °C. Antigen retrieval was performed using EZ-AR antigen retrieval solution 2 (#HX032YCX-GP, Biogenex) at 98 °C for 20 minutes and cooled at 20-25 °C for 10 minutes. Nonspecific binding sites were blocked for 20 minutes at 20-25 °C. Primary antibodies were incubated overnight at 4 °C. Secondary antibodies were incubated at 20-25 °C for 30 minutes. Horseradish peroxidase-conjugated antibodies were visualized using NovaRED chromogen (#SK-4805, Vector). Coverslips were

bioRxiv preprint doi: https://doi.org/10.1101/2025.11.19.689269; this version posted November 19, 2025. The copyright holder for this preprint (which was not certified by peer review) is the author/funder, who has granted bioRxiv a license to display the preprint in perpetuity. It is made available under aCC-BY 4.0 International license.

applied for histology and IHC stains using Permount (#SP-15, Fisher Scientific). For co-IF stains, autofluorescence was quenched using TrueVIEW (#SP-8400-15, Vector), and coverslips were applied using VECTASHIELD mounting medium with DAPI (#H-1200-10, Vector). Images of histological staining and immunostaining were captured using an Axioscan Z1 or 7 (Zeiss) and imaged using ZEN v3.1 blue edition (Zeiss).

Quantification of histology and immunostaining

Complete mid-ventricular heart images were quantified using RGB color thresholds in NIS-Elements AR (v5.11, Nikon). Positive staining area was normalized to tissue area, defined by total pixels – white background pixels. Specific RGB thresholds are listed in the Supplementary Materials Major Resources Tables.

Bulk RNA sequencing

Cold saline (8-10 mL) was perfused from the left ventricle following euthanasia and hearts were harvested immediately. Mid-ventricular sections approximately 1 mm in width were excised using a cold dissection block, rapidly imaged using a Nikon SMZ 25 stereoscope (Nikon), and snap-frozen in liquid nitrogen. RNA was extracted using Maxwell RSC simplyRNA Tissue Kits (#AS1340, Promega) according to the manufacturer's protocol. Samples were processed individually for bulk RNA sequencing, with single mice representing independent experimental replicates. RNA samples were sequenced by Novogene. The sequencing library was generated from total mRNA (1 μg) using NEBNext Ultra™ RNA Library Prep Kits for Illumina (New England BioLabs). cDNA libraries were then sequenced by a Next Generation NovaSeq platform (HWI-ST1276, Illumina, USA), in a pair-end fashion to reach more than 1,500,000 reads. FASTQ sequence data were mapped to the reference mouse genome using HISAT2 (v2.2.1) and quantified using featureCounts (v2.0.6).

Bulk RNA sequencing data were analyzed on R (v4.5.1) (24). Ensembl gene identifiers with no detected read counts in any sample were excluded. Read count data were normalized using the TMM method in the edgeR package (v4.6.3) (25) to adjust for biases in library size and composition. Multi-group comparisons were made using "glmLRT" with hemorrhage presence as a binary covariate in edgeR (25). Since the present study aimed to profile genes with a high potential for forming pathology in AngII-infused mice, miscellaneous transcripts such as duplicated, unnamed, ribosomal, and mitochondrial genes were removed. Criteria for removal was based on searches within Ensembl gene identifiers for "NA," duplicated identifiers, or identifiers containing: "Gm[0 – 9]," "[0 – 9]Rik," "RP[2 – 9]," or "mt-." Gene set enrichment analysis (GSEA) of mouse ortholog Hallmark gene sets was performed using the fgsea package (v1.34.2) on ranked genes (26). Ranks were computed as the sign of the log fold change multiplied by the square root of the likelihood ratio from the interaction model, with sets filtered to 10-500 genes. Mouse ortholog Hallmark gene sets were retrieved from MSigDB with the msigdbr package (v25.1.1) (27). The Benjamini–Hochberg method was used for multiple testing correction and adjusted $p<0.05$ was considered statistically significant. Chord plot illustration was performed using the SRplot online tool (28).

bioRxiv preprint doi: https://doi.org/10.1101/2025.11.19.689269; this version posted November 19, 2025. The copyright holder for this preprint (which was not certified by peer review) is the author/funder, who has granted bioRxiv a license to display the preprint in perpetuity. It is made available under aCC-BY 4.0 International license.

Statistical analysis

Data are presented as median and 25th/75th percentiles in boxes and 5^{th}/95^{th} percentiles in whiskers, with adjacent dots representing outliers. Down triangles or circles represent biological replicates. Statistical analyses for all measurements excepting bulk RNA sequencing were performed using SigmaPlot (v15.0, SYSTAT Software). Normality and homogeneity of variance were assessed by Shapiro–Wilk and Brown–Forsythe tests, respectively. Log, inverse, or Box–Cox transformations were applied to data failing normality and Shapiro–Wilk and Brown–Forsythe tests were repeated. For independent measurements with confirmed normal distribution before or after transformation: homoscedastic and heteroscedastic data were analyzed by Student's and Welch's *t* tests, respectively. Data failing tests for normality and homogeneity of variance were analyzed by Mann-Whitney U test. For repeated measurements, all data met assumptions for normality and homogeneity of variance either before or after transformation and were analyzed by two-way repeated measures ANOVA. $p \leq 0.05$ was considered statistically significant.

Sex as a biological variable

For 1 and 4-week infusion pathological studies, both male and female animals were examined, and similar findings were reported for both sexes. Since no apparent sexual dimorphism was observed in AngII or NE-induced pathology, only male mice were examined for the 1-week bulk RNA sequencing and 1-day AngII infusion studies.

Study approval

All experiments were performed according to a protocol approved by the Institutional Animal Care and Use Committee at the University of Kentucky (Protocol #2018-2967) in accordance with the guidelines of the National Institutes of Health.

Data availability

RNA sequencing data (raw FASTQ and aligned data) will be made publicly available at the gene expression omnibus (GEO) repository. Numerical data that support the findings of this study are provided in the Supporting Data Values file. The data that support the findings of this study are also available from the corresponding authors on reasonable request.

bioRxiv preprint doi: https://doi.org/10.1101/2025.11.19.689269; this version posted November 19, 2025. The copyright holder for this preprint (which was not certified by peer review) is the author/funder, who has granted bioRxiv a license to display the preprint in perpetuity. It is made available under aCC-BY 4.0 International license.

RESULTS

PAI-1 deficiency failed to alter ascending thoracic aortic aneurysm (ATAA) in mice

AngII infusion induces ascending aortic dilatation in mice, recapitulating multiple pathological features of ATAA (29). Our previous work demonstrated that PAI-1 protein abundance was increased markedly in the ascending aortas of mice infused with AngII for 3 days, a stage before overt pathology. Of clinical relevance, PAI-1 was also highly abundant in human ATAA tissue (30). To determine whether PAI-1 contributes to ATAA, AngII was infused for 4 weeks in both male and female PAI-1-/- and their PAI-1+/+ littermates starting at 8-14 weeks of age (Figure 1A). Despite the increased abundance of PAI-1 in thoracic aortas during aneurysm formation (30), its absence did not alter AngII-induced ATAA. No difference was detected between genotypes in ascending aortic diameters, as measured both in live animals by ultrasound (Figure 1B) and *in situ* at termination (Figure 1C). To assess whether PAI-1 deficiency influenced AngII-induced aortic wall remodeling, ascending and descending thoracic aortas were stained for collagen and elastin. Collagen deposition and elastin fragmentation were not changed between PAI-1+/+ and -/- mice infused with AngII (Figure 1, D and E).

PAI-1 deficiency augmented AngII-induced cardiac fibrosis and led to ferric iron deposition

While investigating the contribution of PAI-1 to ATAA, grossly evident cardiac remodeling was observed in both male and female AngII-infused PAI-1-/- mice (Figure 2, A and B). Histological examination of mid-ventricular sections demonstrated increased cardiac collagen deposition in PAI-1-/- mice in patterns consistent with both interstitial and replacement fibrosis. Collagen was localized primarily to the epicardium of both ventricles and the posterior septum. Myocardial fibrosis was also present consistently but distributed heterogeneously. In contrast, perivascular fibrosis, while independent of epicardial involvement, was not apparently altered by PAI-1 deficiency. Quantification of Masson's trichrome staining confirmed that PAI-1 deficiency augmented cardiac fibrosis in AngII-infused mice (Figure 2C).

Given the role of PAI-1 in hemostasis, ferric oxide deposition was examined as a marker of prior hemorrhage. PAI-1-/- mice exhibited ferric iron deposition in regions spatially associated with collagen accumulation, particularly within the epicardium. In contrast, ferric iron was barely detected in PAI-1+/+ mice. Quantification of Prussian blue staining confirmed that PAI-1 deficiency markedly increased ferric iron deposition (Figure 2D).

To investigate whether PAI-1 deficiency augments fibrosis or promotes ferric iron deposition in other highly vascularized organs, tissue sections were examined from the lung, liver, and kidney. Previous studies have reported that PAI-1 deficiency reduces fibrosis in these organs under pathological conditions (6). No differences were detected in collagen deposition between PAI-1+/+ and -/- mice (Supplemental Figure 1, A-C).

bioRxiv preprint doi: https://doi.org/10.1101/2025.11.19.689269; this version posted November 19, 2025. The copyright holder for this preprint (which was not certified by peer review) is the author/funder, who has granted bioRxiv a license to display the preprint in perpetuity. It is made available under aCC-BY 4.0 International license.

Similarly, no apparent ferric iron deposition was detected in either genotype within serial tissue sections of lung, liver, and kidney (Supplemental Figure 2, A-C). These findings suggest that the PAI-1 deficiency exacerbates AngII-induced fibrosis and promotes ferric iron deposition predominantly in the heart.

To determine whether PAI-1 deficiency alone was sufficient to induce cardiac pathology, 8 to 14-week-old male and female mice were infused with saline (the vehicle of AngII) for 4 weeks (Supplemental Figure 3A). Cardiac remodeling, determined by gross examination and Masson's trichrome staining, was not evident in PAI-1-/- mice (Supplemental Figure 3, B and C). Furthermore, cardiac ferric iron deposition was not evident in either genotype (Supplemental Figure 3D). These data demonstrate that PAI-1 deficiency does not induce cardiac pathology under basal conditions, but markedly augments cardiac fibrosis and induces ferric iron deposition in response to AngII infusion.

PAI-1 deficiency did not affect systolic function during AngII infusion

The extent of hypertension-induced cardiac remodeling in PAI-1-/- mice prompted us to investigate whether PAI-1 deficiency also impaired cardiac function. Therefore, male and female mice were infused with either saline or AngII and cardiac morphometry, systolic function, and wall strain were measured by echocardiography at baseline and during 1 and 4 weeks of infusion (Supplemental Figure 4A). No alterations were detected due to the interaction of group and infusion time in left ventricular internal diameter, calculated left ventricular mass, left ventricular anterior wall thickness, ejection fraction, or global longitudinal or circumferential strain. Modest increases in left ventricular posterior wall thickness were detected in male and female PAI-1-/- mice infused with AngII by interaction analysis (Supplemental Figure 4, B and C). Overall, despite the pronounced cardiac pathology in PAI-1-/- mice, no significant differences were discerned in systolic function or wall strain at the intervals studied.

PAI-1 deficiency induced cardiac fibrosis and ferric iron deposition in norepinephrine-infused mice

Infusion of AngII at a rate of 1,000 ng/kg/min increases systolic blood pressure in mice (31-33). To evaluate whether hypertension, per se, promotes cardiac remodeling observed in AngII-infused PAI-1-/- mice, both male and female mice at 11-12 weeks of age were infused with a pressor dose of norepinephrine (NE) for 4 weeks (Figure 3A). Gross cardiac remodeling was evident in PAI-1-/- mice, irrespective of sex, after 4 weeks of NE infusion (Figure 3B). PAI-1+/+ mice exhibited minimal cardiac collagen deposition following NE infusion. In contrast, PAI-1-/- mice displayed interstitial and replacement fibrosis, particularly within the epicardium and posterior septum, but modest perivascular collagen accumulation. Quantification of collagen deposition confirmed that PAI-1 deficiency induced marked cardiac fibrosis (Figure 3C). Ferric iron deposition was detected in PAI-1-/- mice in spatial association with collagen deposition, and quantification of ferric iron staining confirmed its increased abundance (Figure 3D).

bioRxiv preprint doi: https://doi.org/10.1101/2025.11.19.689269; this version posted November 19, 2025. The copyright holder for this preprint (which was not certified by peer review) is the author/funder, who has granted bioRxiv a license to display the preprint in perpetuity. It is made available under aCC-BY 4.0 International license.

PAI-1 deficiency induced cardiac hemorrhage and fibrosis after 1 week of AngII or NE infusion

To determine early pathological events associated with cardiac remodeling in PAI-1-/- mice, both male and female PAI-1+/+ and -/- mice at 11-12 weeks of age were infused with AngII for 1 week (Figure 4A), an interval associated with acute aortic pathology (29). Grossly evident cardiac hemorrhage was observed in PAI-1-/- mice, whereas hemorrhage was barely detectable in PAI-1+/+ mice (Figure 4B). Immuno-histochemical staining for TER-119, a marker of erythrocytes, demonstrated extensive cardiac hemorrhage in PAI-1-/- mice, most pronounced within the epicardium and also present within the myocardium. Quantification of TER-119-positive area confirmed the increased hemorrhage in PAI-1-/- mice (Figure 4C). This early pathological event was associated spatially with the augmented epicardial fibrosis observed after 4 weeks of AngII infusion.

One week of AngII infusion also resulted in significant cardiac fibrosis in PAI-1-/- mice. Collagen deposition was observed predominantly in the myocardium, particularly within the posterior septum. Quantification of Masson's trichrome staining confirmed augmented cardiac fibrosis in PAI-1-/- mice (Figure 4D).

The above findings were also confirmed in both male and female mice infused with NE for 1 week (Figure 5A). NE-infused PAI-1-/- mice developed grossly evident cardiac hemorrhage, while no visible hemorrhage was detected in PAI-1+/+ mice (Figure 5B). The distribution of hemorrhage, as detected by TER-119 staining, was predominantly within the epicardium and myocardium, consistent with the distribution in PAI-1-/- mice infused with AngII for 1 week. Quantification of the TER-119-positive area verified the increased hemorrhage in PAI-1-/- mice (Figure 5C). Masson's trichrome staining revealed that collagen deposition in PAI-1-/- mice was localized mainly to the myocardium, including the posterior septum, a distribution similar to mice infused with AngII for 1 week. Quantification of collagen-positive area demonstrated increased fibrosis in PAI-1-/- mice after 1 week of NE infusion (Figure 5D).

PAI-1 deficiency increased transcripts related to proteolysis and fibrosis independently of hemorrhage severity after 1 week of AngII infusion

To determine the transcriptional alterations associated with cardiac pathology in PAI-1-/- mice, male PAI-1+/+ and -/- mice were infused with saline or AngII for 1 week. Since both male and female PAI-1-/- mice displayed increased cardiac hemorrhage and fibrosis in response to hypertension, only male mice were used. Midventricular tissue sections were analyzed by bulk RNA-sequencing. Among PAI-1-/- mice infused with AngII, 3 mice displayed modest hemorrhage within the sequenced sample, while 7 mice showed pronounced hemorrhage (Supplemental Figure 5A). To avoid complicated data interpretation due to ranges of hemorrhage severity, the presence of prominent hemorrhage was used as a binary covariate in the RNA sequencing analysis, which detected 34,196 genes.

bioRxiv preprint doi: https://doi.org/10.1101/2025.11.19.689269; this version posted November 19, 2025. The copyright holder for this preprint (which was not certified by peer review) is the author/funder, who has granted bioRxiv a license to display the preprint in perpetuity. It is made available under aCC-BY 4.0 International license.

Principal component analysis using unfiltered transcriptomes revealed distinct alterations in AngII-infused mice compared to saline infusion. Within AngII-infused mice, PAI-1-/- mice displayed further transcriptomic alteration from baseline compared to PAI-1+/+ mice (Supplemental Figure 5B). Interaction analysis between infusion and genotype detected 82 differentially expressed genes (DEGs). Hierarchical clustering identified 5 distinct gene clusters (Supplemental Figure 5C). DEGs within cluster #1 were downregulated the most within AngII-infused PAI-1-/- mice. Cluster #2 was comprised of genes upregulated within AngII-infused PAI-1+/+ mice. DEGs within cluster #3 displayed increased expression coincident with significant hemorrhage presence in AngII-infused PAI-1-/- mice. Cluster 4 contained a single gene, *C1qtnf3*, that was highly expressed within AngII-infused PAI-1-/- mice with modest hemorrhage (Supplemental Figure 5D). The largest number of DEGs were grouped within cluster #5; these genes were highly abundant in AngII-infused PAI-1-/- mice, irrespective of hemorrhage severity.

To identify individual transcripts with a high potential for forming pathology in AngII-infused PAI-1-/- mice, the differential expression analysis was integrated with gene set enrichment analysis focused on mouse ortholog Hallmark gene sets. Among the top 10 Hallmark gene sets with positive enrichment scores, 12 DEGs were present within the leading edge of the gene sets (Supplemental Figure 6A). All 12 DEGs were present within cluster #5. Additionally, 6 of the 12 DEGs were present within at least two Hallmark gene sets and encoded for ECM components (*Fn1* and *Ecm1*), proteases (*Lgals3* and *Ctss*), a polyamine catabolic enzyme (*Sat1*), or an immune-stimulatory receptor (*Cd48*, Supplemental Figure 6B). These findings suggest that PAI-deficient hearts exhibit transcriptional signatures of injury and remodeling in response to AngII infusion for 1 week, even in the absence of severe hemorrhage.

PAI-1 deficiency augmented cardiac hemorrhage and myocyte loss within 1 day of AngII infusion

PAI-1 deficiency promoted both fibrosis and hemorrhage after 1 week of AngII or NE infusion. To determine whether hemorrhage occurs rapidly, 9 to 12-week-old mice were infused with AngII for 1 day (Figure 6A). Since both male and female PAI-1-/- mice displayed increased cardiac hemorrhage and fibrosis in response to AngII infusion for 1 and 4 weeks, only male mice were infused for the 1-day interval. Grossly evident cardiac hemorrhage was detected in the posterior wall of PAI-1-/- mice, while hemorrhage was barely visible in PAI-1+/+ mice (Figure 6B). Staining for erythrocytes revealed diffuse hemorrhage localized within the myocardium and posterior septum of PAI-1-/- mice (Figure 6C). This distribution of hemorrhage was consistent with the distribution of collagen accumulation in PAI-1-/- mice after 1 week of AngII infusion. Quantification of TER-119-positive area confirmed the augmentation of hemorrhage in PAI-1-/- mice (Figure 6C).

Cardiomyocyte loss was observed at 1 day of AngII infusion (Figure 6). Therefore, staining for cardiac troponin I, a marker of cardiomyocytes, was performed. Restricted areas of nucleated, non-vascular, troponin I-negative myocardium were

bioRxiv preprint doi: https://doi.org/10.1101/2025.11.19.689269; this version posted November 19, 2025. The copyright holder for this preprint (which was not certified by peer review) is the author/funder, who has granted bioRxiv a license to display the preprint in perpetuity. It is made available under aCC-BY 4.0 International license.

observed in PAI-1+/+ mice, consistent with minor cardiomyocyte injury (Supplemental Figure 7). In contrast, cardiomyocyte injury was evident prominently in PAI-1-/- mice, particularly within the posterior septum and myocardium. Serial staining of TER-119 and troponin I indicated that areas of cardiomyocyte injury in PAI-1-/- mice coincided predominantly with hemorrhage (Figure 6C and Supplemental Figure 7). To verify that TER-119 accumulation in PAI-1-/- mice was representative of hemorrhage, co-immunofluorescent (co-IF) staining was performed for nuclei (4',6-diamidino-2-phenylindole, DAPI), endothelium (CD31), and erythrocytes (TER-119). Erythrocytes within the myocardium of PAI-1-/- mice were accumulated outside of vessel lumens, indicative of tissue hemorrhage (Supplemental Figure 8, A and B).

bioRxiv preprint doi: https://doi.org/10.1101/2025.11.19.689269; this version posted November 19, 2025. The copyright holder for this preprint (which was not certified by peer review) is the author/funder, who has granted bioRxiv a license to display the preprint in perpetuity. It is made available under aCC-BY 4.0 International license.

DISCUSSION

The primary objective of this study was to assess the role of PAI-1 in AngII-induced ATAA. PAI-1 deficiency, however, did not affect ascending aortic dilatation or vascular pathologies after 4 weeks of AngII infusion. Instead, cardiac fibrosis was observed in PAI-1-/- mice in response to AngII infusion. While this finding has been reported previously (8, 11-13), our studies, with detailed spatial and temporal exploration, revealed several novel observations: (1) PAI-1 deficiency augmented cardiac fibrosis and promoted ferric iron deposition in both AngII- and NE-infused mice, regardless of sex; (2) PAI-1 deficiency triggered cardiac hemorrhage and cardiomyocyte loss as early as 1 day of AngII infusion; and (3) hemorrhage observed at 1 day and 1 week infusion intervals spatially coincided with augmented fibrosis observed at 1 and 4 week intervals, respectively.

Despite the abundance of PAI-1 in human ATAA and ascending aortas of AngII-infused mice (30), its deficiency did not alter AngII-induced aortic dilatation or remodeling. This outcome differs from reports of reduced aortic remodeling in AngII-infused PAI-1-/- mice (8, 13). In addition to the aorta, PAI-1 deficiency did not change coronary perivascular fibrosis after 4 weeks of AngII or NE infusion in our study, differing from the protective effect of PAI-1 deficiency against Nω-Nitro-L-arginine methyl ester (L-NAME)-induced perivascular fibrosis (34, 35). These discrepancies likely reflect the distinct vascular stresses and stimuli induced by different models of hypertension (36). Additional variables such as age at study onset, AngII infusion strategy, and strain differences may influence the impact of PAI-1 deficiency on vascular remodeling.

In the heart, extensive fibrosis was observed in PAI-1-/- mice after 1 or 4 weeks of AngII or NE infusion, consistent with previous reports in AngII-infused mice (8, 11-13). Our studies exhibited that PAI-1 deficiency augmented cardiac fibrosis regardless of sex, whereas analysis stratified by sex has not been reported previously. In the present study, 8 to 14-week-old mice were used, which exhibited no detectable cardiac fibrosis in the absence of AngII or NE infusion, replicating previous work in mice within 6 months of age (9, 13). However, spontaneous cardiac fibrosis has been reported in 9 to 24-month-old PAI-1-/- mice (7, 9, 10). These data reveal a remarkable contrast: PAI-1 deficiency alone induces gradual cardiac fibrosis that is only manifest at advanced age, whereas infusions with either AngII or NE generate dramatic pathology within 1 to 4 weeks. To determine the associated functional consequences, we performed longitudinal echocardiography during AngII infusion. PAI-1-/- mice had increased posterior wall thickness, consistent with previously reported hypertrophy (13). Systolic function was unchanged by PAI-1 deficiency, contrasting with the reduced ejection fraction reported after 2 weeks of AngII followed by 2 weeks without infusion in 16 to 20-week-old mice (13). Differences in age at study onset and AngII infusion intervals may influence the susceptibility of PAI-1-/- mice to AngII-induced systolic dysfunction. Overall, our findings demonstrate that hypertension induced cardiac fibrosis and modest

bioRxiv preprint doi: https://doi.org/10.1101/2025.11.19.689269; this version posted November 19, 2025. The copyright holder for this preprint (which was not certified by peer review) is the author/funder, who has granted bioRxiv a license to display the preprint in perpetuity. It is made available under aCC-BY 4.0 International license.

alterations in ventricular wall thickness without detectable impairment of systolic function.

Either in aged (7, 9, 10) or AngII-infused mice (8, 11-13), PAI-1 deficiency does not induce fibrosis in the lung, liver, or kidney. Therefore, the acceleration of fibrosis appears to be unique to the hearts of PAI-1-/- mice. The heart is a highly muscular organ that constantly contracts to propel blood to the circulatory system, exposing it to substantial mechanical load. Given that both AngII and NE, two molecules well known to increase blood pressure, exacerbate cardiac fibrosis in PAI-1-/- mice, a plausible accelerating mechanism is constant hemodynamic mechanical stress. Such stress may promote microinjury and amplify fibrotic signaling cascades in cardiac tissue lacking PAI-1, ultimately precipitating the pronounced fibrotic remodeling observed in these mice.

To further understand the potential mechanisms by which PAI-1 accelerates AngII-augmented cardiac fibrosis in mice, AngII was infused for either 1 or 7 days. These investigations in early infusion intervals of either AngII or NE build upon prior reports of cardiac fibrosis in PAI-1 deficiency (7-13) by identifying hemorrhage and myocyte injury as preceding events. PAI-1-/- mice displayed diffuse posterior septal and myocardial hemorrhage and myocyte loss after only 1 day of AngII infusion. After 1 week of AngII or NE infusion, PAI-1-/- mice displayed primarily replacement fibrosis within the myocardium and posterior septum as well as diffuse epicardial hemorrhage. Transcriptomic profiling after 1 week of AngII revealed elevations in fibrotic and proteolytic transcripts independent of hemorrhage, consistent with pathway-level results reported previously (13). By 4 weeks of AngII or NE infusion, PAI-1-/- mice displayed predominant epicardial replacement fibrosis, in addition to myocardial and posterior septal fibrosis. Ferric iron deposition was coincident with locations of fibrosis, resembling findings in aged mice or young adult mice co-administered with AngII and aldosterone (9, 12). Of note, this phenotype has not been reported previously in mice receiving infusions of either NE or AngII. The predominantly epicardial distribution of injury resembles that seen in aged low-tissue-factor or low-factor VII mice (37) and in cardiomyocyte-specific tissue factor-deficient mice exposed to isoproterenol (38). Such regional injury and our observations of diffuse hemorrhage likely reflect microvascular susceptibility to hemodynamic stress. AngII and NE infusion produced similar pathologies in PAI-1-/- mice after 1 and 4 weeks of infusion, indicating that hemodynamic stress itself, rather than hormone-specific signaling, drives the phenotype, paralleling a report of increased cardiac fibrosis in cardiomyocyte-specific PAI-1-/- mice after transverse aortic constriction (39). These results highlight the unique vulnerability of the heart to stress-induced microvascular damage. Observations of hemorrhage being spatially coincident with subsequent fibrosis implicate microvascular instability as a driver of cardiac injury in PAI-1-/- mice.

PAI-1 is a multifunctional serine protease inhibitor that reduces plasmin-mediated fibrinolysis and extracellular proteolysis through inhibition of plasminogen activators via its reactive center-loop (RCL) (4, 18, 40). PAI-1 also exerts several plasmin-

bioRxiv preprint doi: https://doi.org/10.1101/2025.11.19.689269; this version posted November 19, 2025. The copyright holder for this preprint (which was not certified by peer review) is the author/funder, who has granted bioRxiv a license to display the preprint in perpetuity. It is made available under aCC-BY 4.0 International license.

independent effects as a regulator of cell adhesion, migration, and angiogenesis via domains distinct from its RCL (41, 42). In contrast to its effect in the heart, PAI-1 often promotes organ fibrosis (6); PAI-1 mutational studies have demonstrated that it promotes lung fibrosis independently of its RCL (43, 44). Prior reports have implicated uPA and plasmin-mediated activation of transforming growth factor-β as key drivers of cardiac microvascular injury and fibrosis in PAI-1 deficiency (12, 13). Collectively, these data suggest that the cardioprotective effects of PAI-1 stem primarily from RCL-mediated inhibition of plasminogen activators. Future studies using domain-specific loss-of-function mutants will be essential to define how its distinct structural regions influence cardiac vascular and fibrotic responses to hypertension.

In summary, this study demonstrated that PAI-1 deficiency promoted hypertension-induced cardiac hemorrhage and fibrosis triggered by two distinct stimuli. Spatial, temporal, and molecular analyses support a model in which microvascular hemorrhage and cardiomyocyte loss precede fibrotic remodeling in the absence of PAI-1. These findings underscore a critical role for PAI-1 in preserving cardiac microvascular integrity under hemodynamic stress and highlight potential structure-function relationships that warrant further investigation. In agreement with these experimental studies, cardiac fibrosis has also been reported in a human population with PAI-1 deficiency (13, 45), highlighting the clinical relevance of the phenotype observed in mice. Cardiac fibrosis resulting from PAI-1 deficiency currently lacks targeted therapy. Our findings suggest that these patients may be intrinsically susceptible to hemodynamic stress-induced cardiac microvascular injury. Approaches aimed at minimizing elevations in blood pressure, promoting endothelial stability, or reducing plasmin activity could therefore represent additional therapeutic strategies.

bioRxiv preprint doi: https://doi.org/10.1101/2025.11.19.689269; this version posted November 19, 2025. The copyright holder for this preprint (which was not certified by peer review) is the author/funder, who has granted bioRxiv a license to display the preprint in perpetuity. It is made available under aCC-BY 4.0 International license.

FUNDING SUPPORT

This research work is supported by the National Institutes of Health (R35HL155649 and TL1TR001997) and a MERIT award from the American Heart Association (23MERIT1036341). The content in this article is solely the responsibility of the authors and does not necessarily represent the official views of the National Institutes of Health.

AUTHOR CONTRIBUTIONS

Conceptualization: ACP, HS, JES, HSL, AD

Data curation: ACP, SI, HS, HSL, AD

Formal analysis: ACP, DBG, VZG, NZ, HS, JES

Funding acquisition: ACP, AD

Investigation: ACP, SI, MKF, DAH, JJM, BML, DBG, VZG, NZ, JES

Methodology: ACP, HS, HSL, AD

Project administration: HSL, AD

Writing–original draft: ACP

Writing–review & editing: SI, MKF, DAH, JJM, BML, DBG, VZG, NZ, HS, JES, HSL, AD

ACKNOWLEDGMENTS

None

CONFLICT OF INTEREST

The authors declare they have no conflicts of interest.

bioRxiv preprint doi: https://doi.org/10.1101/2025.11.19.689269; this version posted November 19, 2025. The copyright holder for this preprint (which was not certified by peer review) is the author/funder, who has granted bioRxiv a license to display the preprint in perpetuity. It is made available under aCC-BY 4.0 International license.

REFERENCES

1. Roth GA, Mensah GA, Johnson CO, Addolorato G, Ammirati E, Baddour LM, et al. Global burden of cardiovascular diseases and risk factors, 1990-2019: update from the GBD 2019 study. *J Am Coll Cardiol.* 2020;76(25):2982-3021.
2. Milewicz DM, and Ramirez F. Therapies for thoracic aortic aneurysms and acute aortic dissections. *Arteriosclerosis, thrombosis, and vascular biology.* 2019;39(2):126-36.
3. Floris E, Cozzolino C, Marconi S, Tonicello F, Picchio V, Pagano F, et al. A review of therapeutic strategies against cardiac fibrosis: from classical pharmacology to novel molecular, epigenetic, and biotechnological approaches. *Rev Cardiovasc Med.* 2023;24(8):226.
4. Cale JM, and Lawrence DA. Structure-function relationships of plasminogen activator inhibitor-1 and its potential as a therapeutic agent. *Curr Drug Targets.* 2007;8(9):971-81.
5. Sillen M, and Declerck PJ. Targeting PAI-1 in cardiovascular disease: Structural insights into PAI-1 functionality and inhibition. *Front Cardiovasc Med.* 2020;7:622473.
6. Ghosh AK, and Vaughan DE. PAI-1 in tissue fibrosis. *J Cell Physiol.* 2012;227(2):493-507.
7. Moriwaki H, Stempien-Otero A, Kremen M, Cozen AE, and Dichek DA. Overexpression of urokinase by macrophages or deficiency of plasminogen activator inhibitor type 1 causes cardiac fibrosis in mice. *Circulation research.* 2004;95(6):637-44.
8. Weisberg AD, Albornoz F, Griffin JP, Crandall DL, Elokdah H, Fogo AB, et al. Pharmacological inhibition and genetic deficiency of plasminogen activator inhibitor-1 attenuates angiotensin II/salt-induced aortic remodeling. *Arteriosclerosis, thrombosis, and vascular biology.* 2005;25(2):365-71.
9. Xu Z, Castellino FJ, and Ploplis VA. Plasminogen activator inhibitor-1 (PAI-1) is cardioprotective in mice by maintaining microvascular integrity and cardiac architecture. *Blood.* 2010;115(10):2038-47.
10. Ghosh AK, Bradham WS, Gleaves LA, De Taeye B, Murphy SB, Covington JW, et al. Genetic deficiency of plasminogen activator inhibitor-1 promotes cardiac fibrosis in aged mice. *Circulation.* 2010;122(12):1200-9.
11. Knier B, Cordasic N, Klanke B, Heusinger-Ribeiro J, Daniel C, Veelken R, et al. Effect of the plasminogen-plasmin system on hypertensive renal and cardiac damage. *J Hypertens.* 2011;29(8):1602-12.
12. Gupta KK, Donahue DL, Sandoval-Cooper MJ, Castellino FJ, and Ploplis VA. Plasminogen activator inhibitor-1 protects mice against cardiac fibrosis by inhibiting urokinase-type plasminogen activator-mediated plasminogen activation. *Scientific Reports.* 2017;7(1):365.
13. Flevaris P, Khan SS, Eren M, Schuldt AJT, Shah SJ, Lee DC, et al. Plasminogen activator inhibitor type I controls cardiomyocyte transforming growth factor-β and cardiac fibrosis. *Circulation.* 2017;136(7):664-79.
14. Allaire E, Hasenstab D, Kenagy RD, Starcher B, Clowes MM, and Clowes AW. Prevention of aneurysm development and rupture by local overexpression of plasminogen activator inhibitor-1. *Circulation.* 1998;98(3):249-55.

bioRxiv preprint doi: https://doi.org/10.1101/2025.11.19.689269; this version posted November 19, 2025. The copyright holder for this preprint (which was not certified by peer review) is the author/funder, who has granted bioRxiv a license to display the preprint in perpetuity. It is made available under aCC-BY 4.0 International license.

15. Qian HS, Gu JM, Liu P, Kauser K, Halks-Miller M, Vergona R, et al. Overexpression of PAI-1 prevents the development of abdominal aortic aneurysm in mice. *Gene Ther.* 2008;15:224-32.
16. DiMusto PD, Lu G, Ghosh A, Roelofs KJ, Su G, Zhao Y, et al. Increased PAI-1 in females compared with males is protective for abdominal aortic aneurysm formation in a rodent model. *Am J Physiol Heart Circ Physiol.* 2012;302(7):H1378-86.
17. Zhao M, Hu L, Lin Z, Yue X, Zheng X, Piao M, et al. Plasminogen activator inhibitor 1 controls abdominal aortic aneurysm formation via the modulation of TGF-beta/Smad2/3 signaling in mice. *FASEB J.* 2025;39(9):e70562.
18. Sillen M, and Declerck PJ. A narrative review on plasminogen activator inhibitor-1 and its (patho)physiological role: to target or not to target? *Int J Mol Sci.* 2021;22(5):2721.
19. Percie du Sert N, Hurst V, Ahluwalia A, Alam S, Avey MT, Baker M, et al. The ARRIVE guidelines 2.0: updated guidelines for reporting animal research. *J Physiol.* 2020;598(18):3793-801.
20. Sawada H, Chen JZ, Wright BC, Moorleghen JJ, Lu HS, and Daugherty A. Ultrasound imaging of the thoracic and abdominal aorta in mice to determine aneurysm dimensions. *J Vis Exp.* 2019(145):10.3791/59013.
21. Zacchigna S, Paldino A, Falcao-Pires I, Daskalopoulos EP, Dal Ferro M, Vodret S, et al. Towards standardization of echocardiography for the evaluation of left ventricular function in adult rodents: a position paper of the ESC Working Group on Myocardial Function. *Cardiovasc Res.* 2021;117(1):43-59.
22. Ohno-Urabe S, Kukida M, Franklin MK, Katsumata Y, Su W, Gong MC, et al. Authentication of in situ measurements for thoracic aortic aneurysms in mice. *Arteriosclerosis, thrombosis, and vascular biology.* 2021;41(6):2117-9.
23. Ito S, Lu HS, Daugherty A, and Sawada H. Imaging techniques for aortic aneurysms and dissections in mice: comparisons of ex vivo, in situ, and ultrasound approaches. *Biomolecules.* 2022;12(2):339.
24. Team RC. R: A language and environment for statistical computing. *R Foundation for Statistical Computing.* 2021: https://www.R-project.org/.
25. Robinson MD, McCarthy DJ, and Smyth GK. edgeR: a Bioconductor package for differential expression analysis of digital gene expression data. *Bioinformatics.* 2010;26(1):139-40.
26. Korotkevich G SV, Budin N, Shpak B, Artyomov MN, Sergushichev A. Fast gene set enrichment analysis. *bioRxiv.* 2019.
27. Dolgalev I. Comprehensive R Archive Network (CRAN); 2022.
28. Tang D, Chen M, Huang X, Zhang G, Zeng L, Zhang G, et al. SRplot: A free online platform for data visualization and graphing. *PLoS One.* 2023;18(11):e0294236.
29. Rateri DL, Davis FM, Balakrishnan A, Howatt DA, Moorleghen JJ, O'Connor WN, et al. Angiotensin II induces region-specific medial disruption during evolution of ascending aortic aneurysms. *Am J Pathol.* 2014;184(9):2586-95.
30. Sawada H, Katsumata Y, Higashi H, Zhang C, Li Y, Morgan S, et al. Second heart field-derived cells contribute to angiotensin II-mediated ascending aortopathies. *Circulation.* 2022;145(13):987-1001.

bioRxiv preprint doi: https://doi.org/10.1101/2025.11.19.689269; this version posted November 19, 2025. The copyright holder for this preprint (which was not certified by peer review) is the author/funder, who has granted bioRxiv a license to display the preprint in perpetuity. It is made available under aCC-BY 4.0 International license.

31. Kawada N, Imai E, Karber A, Welch WJ, and Wilcox CS. A mouse model of angiotensin II slow pressor response: role of oxidative stress. *J Am Soc Nephrol.* 2002;13(12):2860-8.
32. Owens AP 3rd, Subramanian V, Moorleghen JJ, Guo Z, McNamara CA, Cassis LA, et al. Angiotensin II induces a region-specific hyperplasia of the ascending aorta through regulation of inhibitor of differentiation 3. *Circulation research.* 2010;106(3):611-9.
33. Gomolak JR, and Didion SP. Angiotensin II-induced endothelial dysfunction is temporally linked with increases in interleukin-6 and vascular macrophage accumulation. *Front Physiol.* 2014;5:396.
34. Kaikita K, Fogo AB, Ma L, Schoenhard JA, Brown NJ, and Vaughan DE. Plasminogen activator inhibitor-1 deficiency prevents hypertension and vascular fibrosis in response to long-term nitric oxide synthase inhibition. *Circulation.* 2001;104(7):839-44.
35. Kaikita K, Schoenhard JA, Painter CA, Ripley RT, Brown NJ, Fogo AB, et al. Potential roles of plasminogen activator system in coronary vascular remodeling induced by long-term nitric oxide synthase inhibition. *J Mol Cell Cardiol.* 2002;34(6):617-27.
36. Jama HA, Muralitharan RR, Xu C, O'Donnell JA, Bertagnolli M, Broughton BRS, et al. Rodent models of hypertension. *Br J Pharmacol.* 2022;179(5):918-37.
37. Pawlinski R, Fernandes A, Kehrle B, Pedersen B, Parry G, Erlich J, et al. Tissue factor deficiency causes cardiac fibrosis and left ventricular dysfunction. *Proc Natl Acad Sci USA.* 2002;99(24):15333-8.
38. Pawlinski R, Tencati M, Holscher T, Pedersen B, Voet T, Tilley RE, et al. Role of cardiac myocyte tissue factor in heart hemostasis. *J Thromb Haemost.* 2007;5(8):1693-700.
39. Ghosh AK, Kalousdian AA, Shang M, Lux E, Eren M, Keating A, et al. Cardiomyocyte PAI-1 influences the cardiac transcriptome and limits the extent of cardiac fibrosis in response to left ventricular pressure overload. *Cell Signal.* 2023;104:110555.
40. Lawrence DA, Ginsburg D, Day DE, Berkenpas MB, Verhamme IM, Kvassman JO, et al. Serpin-protease complexes are trapped as stable acyl-enzyme intermediates. *J Biol Chem.* 1995;270(43):25309-12.
41. Czekay RP, Wilkins-Port CE, Higgins SP, Freytag J, Overstreet JM, Klein RM, et al. PAI-1: an integrator of cell signaling and migration. *Int J Cell Biol.* 2011;2011:562481.
42. Wu J, Strawn TL, Luo M, Wang L, Li R, Ren M, et al. Plasminogen activator inhibitor-1 inhibits angiogenic signaling by uncoupling vascular endothelial growth factor receptor-2-alphaVbeta3 integrin cross talk. *Arteriosclerosis, thrombosis, and vascular biology.* 2015;35(1):111-20.
43. Courey AJ, Horowitz JC, Kim KK, Koh TJ, Novak ML, Subbotina N, et al. The vitronectin-binding function of PAI-1 exacerbates lung fibrosis in mice. *Blood.* 2011;118(8):2313-21.
44. Sisson TH, Osterholzer JJ, Leung L, Basrur V, Nesvizhskii A, Subbotina N, et al. PAI-1 interaction with sortilin-related receptor 1 is required for lung fibrosis. *JCI Insight.* 2025;10(11).

bioRxiv preprint doi: https://doi.org/10.1101/2025.11.19.689269; this version posted November 19, 2025. The copyright holder for this preprint (which was not certified by peer review) is the author/funder, who has granted bioRxiv a license to display the preprint in perpetuity. It is made available under aCC-BY 4.0 International license.

45. Khan SS, Shah SJ, Strande JL, Baldridge AS, Flevaris P, Puckelwartz MJ, et al. Identification of cardiac fibrosis in young adults with a homozygous frameshift variant in SERPINE1. *JAMA Cardiology.* 2021;6(7):841-6.

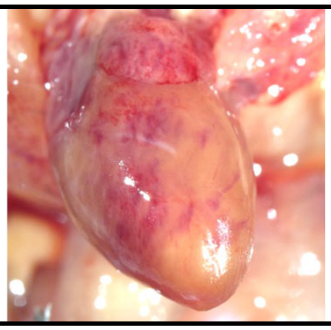
bioRxiv preprint doi: https://doi.org/10.1101/2025.11.19.689269; this version posted November 19, 2025. The copyright holder for this preprint (which was not certified by peer review) is the author/funder, who has granted bioRxiv a license to display the preprint in perpetuity. It is made available under aCC-BY 4.0 International license.

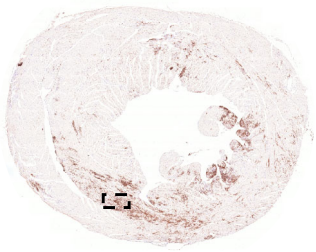
GRAPHIC ABSTRACT

AngII or NE-induced hypertension

PAI-1

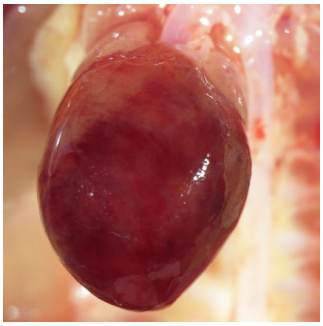
1 day

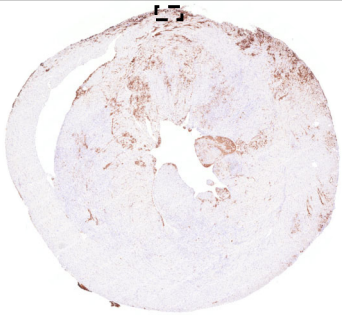


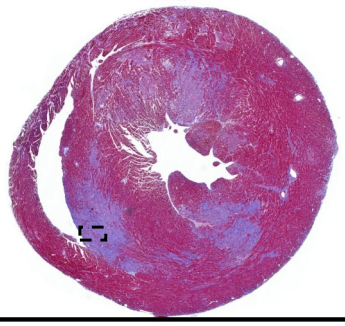


Myocardial hemorrhage

1 week



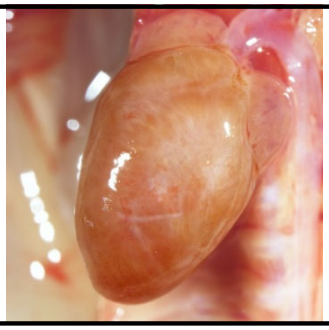


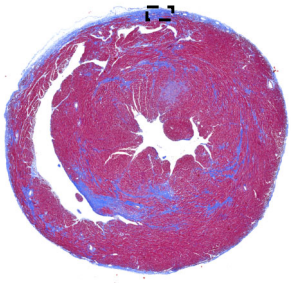


Epicardial hemorrhage

Myocardial fibrosis

4 weeks





Epicardial fibrosis

Erythrocytes (TER-119 Staining) Collagen (Masson's Trichrome)

bioRxiv preprint doi: https://doi.org/10.1101/2025.11.19.689269; this version posted November 19, 2025. The copyright holder for this preprint (which was not certified by peer review) is the author/funder, who has granted bioRxiv a license to display the preprint in perpetuity. It is made available under aCC-BY 4.0 International license.

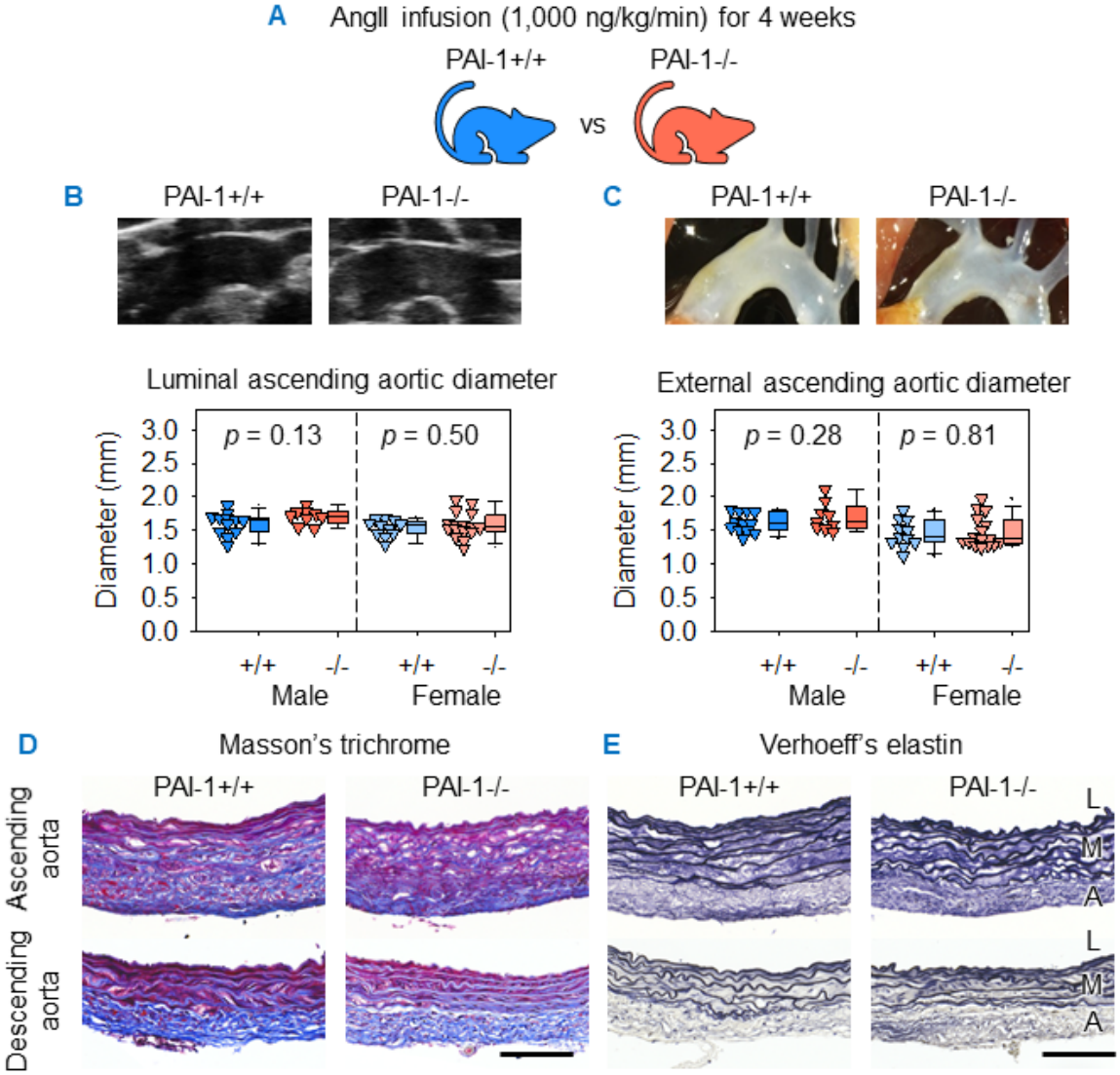


Figure 1. **PAI-1 deficiency failed to alter ascending thoracic aortic aneurysm in mice.** (**A**) Male and female PAI-1+/+ and -/- littermates were infused with AngII (1,000 ng/kg/min) for 4 weeks. (**B**) Representative right parasternal ultrasound images and quantification of maximal luminal ascending aortic diameter measurements. (**C**) Representative *in situ* aortic images and quantification of maximal external aortic diameter measurements. Representative Masson's trichrome (**D**) and Verhoeff's elastin staining (**E**) of ascending and descending aortic sections. Representative images are from male mice. Comparisons between genotypes made by Student's *t* test (**B**) and Student's *t* test for males and Student's *t* test after log transformation for females (**C**). *n* = 9-16 mice/group. Scale bars = 100 μm. Abbreviations: AngII: angiotensin II, PAI-1: plasminogen activator inhibitor-1, L: lumen, M: media, A: adventitia.

bioRxiv preprint doi: https://doi.org/10.1101/2025.11.19.689269; this version posted November 19, 2025. The copyright holder for this preprint (which was not certified by peer review) is the author/funder, who has granted bioRxiv a license to display the preprint in perpetuity. It is made available under aCC-BY 4.0 International license.

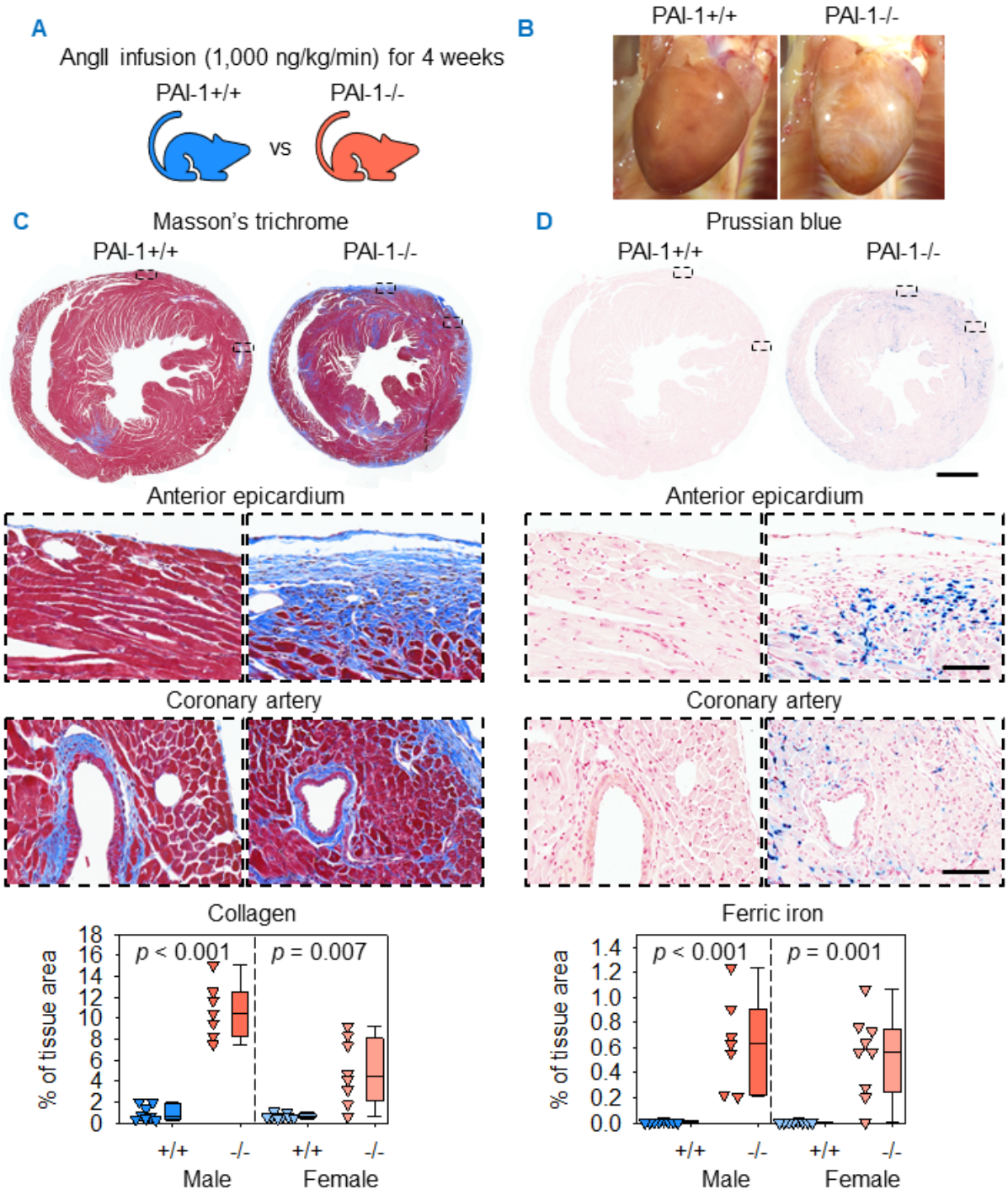


Figure 2. **PAI-1 deficiency augmented AngII-induced cardiac fibrosis and induced ferric iron deposition**. (**A**) Male and female PAI-1+/+ and -/- littermates were infused with AngII (1,000 ng/kg/min) for 4 weeks. (**B**) Representative *in situ* heart images. (**C**) Representative Masson's trichrome staining and collagen quantification of mid-ventricular hearts. Comparisons between genotypes were made by Welch's *t* test. (**D**) Representative Prussian blue staining and ferric iron quantification of mid-ventricular hearts. Comparisons between genotypes were made by Student's *t* test after log transformation for males and Mann-Whitney U test for females. *n* = 7-9 mice/group. Representative images are from male mice. Scale bars = 1,000 μm and 100 μm for low and high-magnification images, respectively. Abbreviations: AngII: angiotensin II, PAI-1: plasminogen activator inhibitor-1.

bioRxiv preprint doi: https://doi.org/10.1101/2025.11.19.689269; this version posted November 19, 2025. The copyright holder for this preprint (which was not certified by peer review) is the author/funder, who has granted bioRxiv a license to display the preprint in perpetuity. It is made available under aCC-BY 4.0 International license.

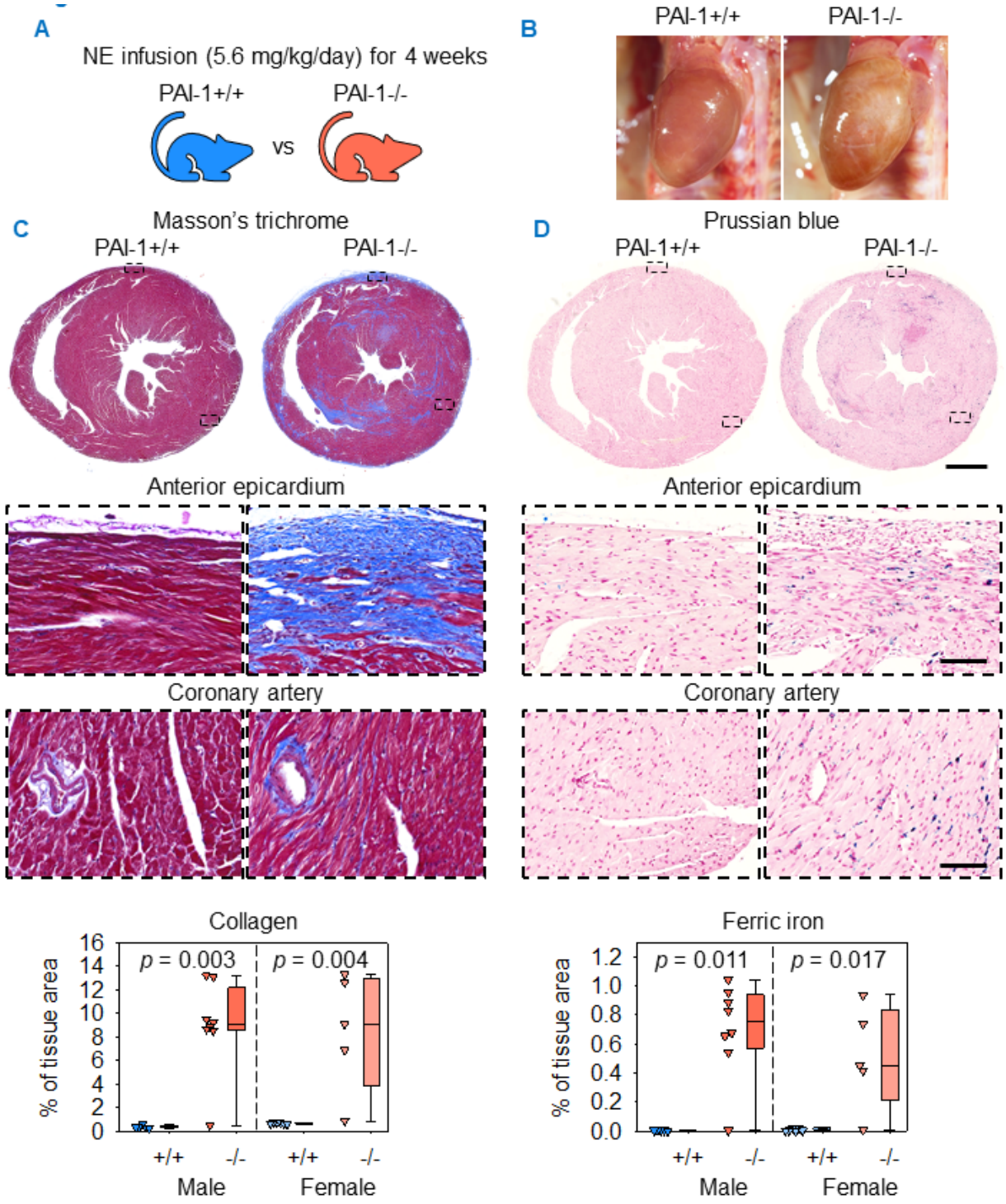


Figure 3. **PAI-1 deficiency induced cardiac fibrosis and ferric iron deposition in NE-infused mice**. (**A**) Male and female PAI-1+/+ and -/- littermates were infused with NE (5.6 mg/kg/day) for 4 weeks. (**B**) Representative *in situ* heart images. Representative Masson's trichrome staining and collagen quantification (**C**) and Prussian blue staining and ferric iron quantification (**D**) of mid-ventricular hearts. Comparisons between genotypes were made by Mann-Whitney U test. *n* = 5-8 mice/group. Representative images are from male mice. Scale bars = 1,000 μm and 100 μm for low and high-magnification images, respectively. Abbreviations: NE: norepinephrine, PAI-1: plasminogen activator inhibitor-1.

bioRxiv preprint doi: https://doi.org/10.1101/2025.11.19.689269; this version posted November 19, 2025. The copyright holder for this preprint (which was not certified by peer review) is the author/funder, who has granted bioRxiv a license to display the preprint in perpetuity. It is made available under aCC-BY 4.0 International license.

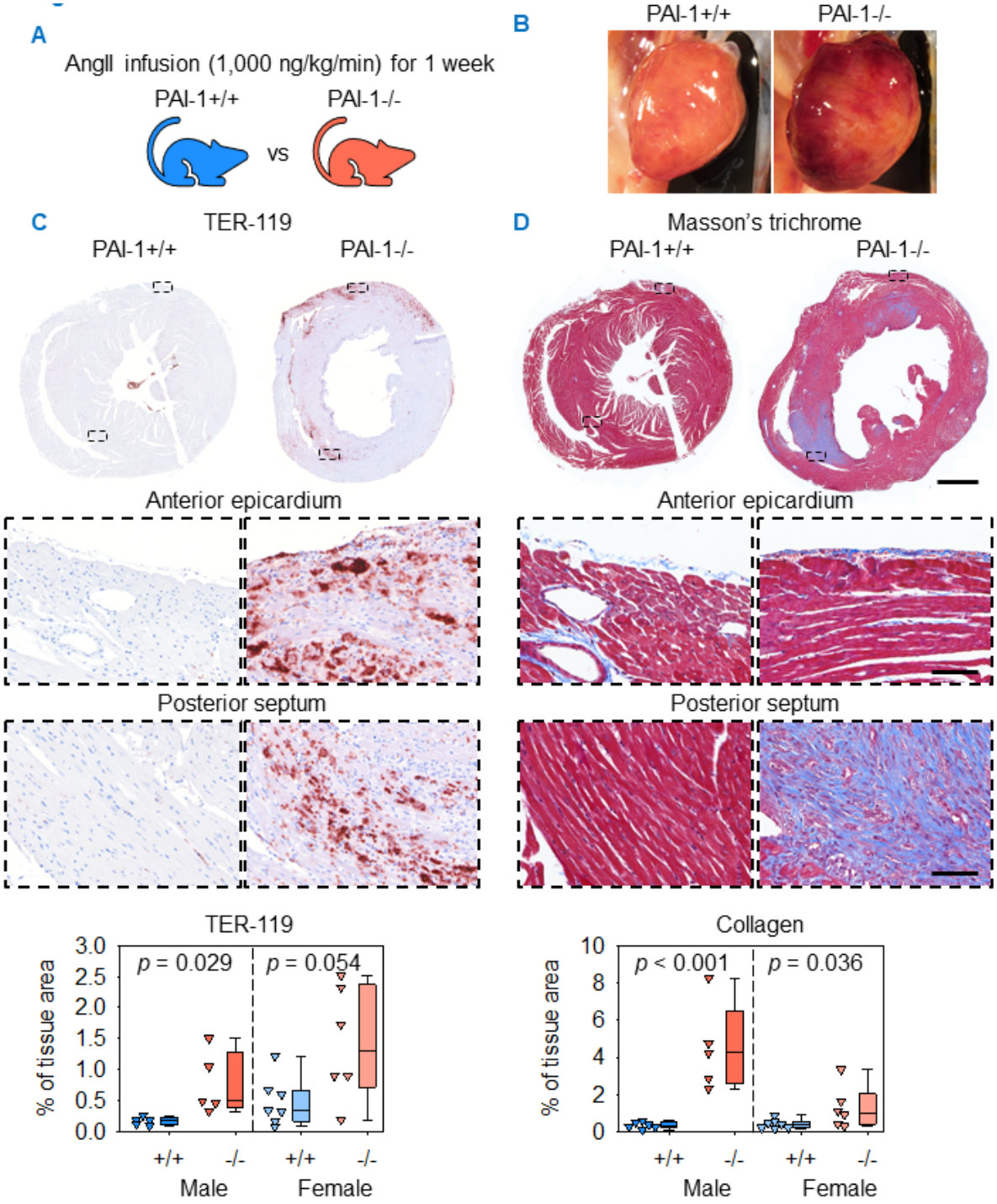


Figure 4. **PAI-1 deficiency augmented AngII-induced cardiac fibrosis and promoted hemorrhage after 1 week of AngII infusion.** (**A**) Male and female PAI-1+/+ and -/- littermates were infused with AngII (1,000 ng/kg/min) for 1 week. (**B**) Representative *in situ* heart images. (**C**) Representative TER-119 immunohistochemistry and quantification of mid-ventricular hearts. Comparisons between genotypes were made by Student's *t* test for males and Welch's *t* test for females. (**D**) Masson's trichrome staining and collagen quantification of mid-ventricular hearts. Comparisons between genotypes were made by Student's *t* test after log transformation. *n* = 5-7 mice/group. Representative images are from male mice. Scale bars = 1,000 μm and 100 μm for low and high-magnification images, respectively. Abbreviations: AngII: angiotensin II, PAI-1: plasminogen activator inhibitor-1.

bioRxiv preprint doi: https://doi.org/10.1101/2025.11.19.689269; this version posted November 19, 2025. The copyright holder for this preprint (which was not certified by peer review) is the author/funder, who has granted bioRxiv a license to display the preprint in perpetuity. It is made available under aCC-BY 4.0 International license.

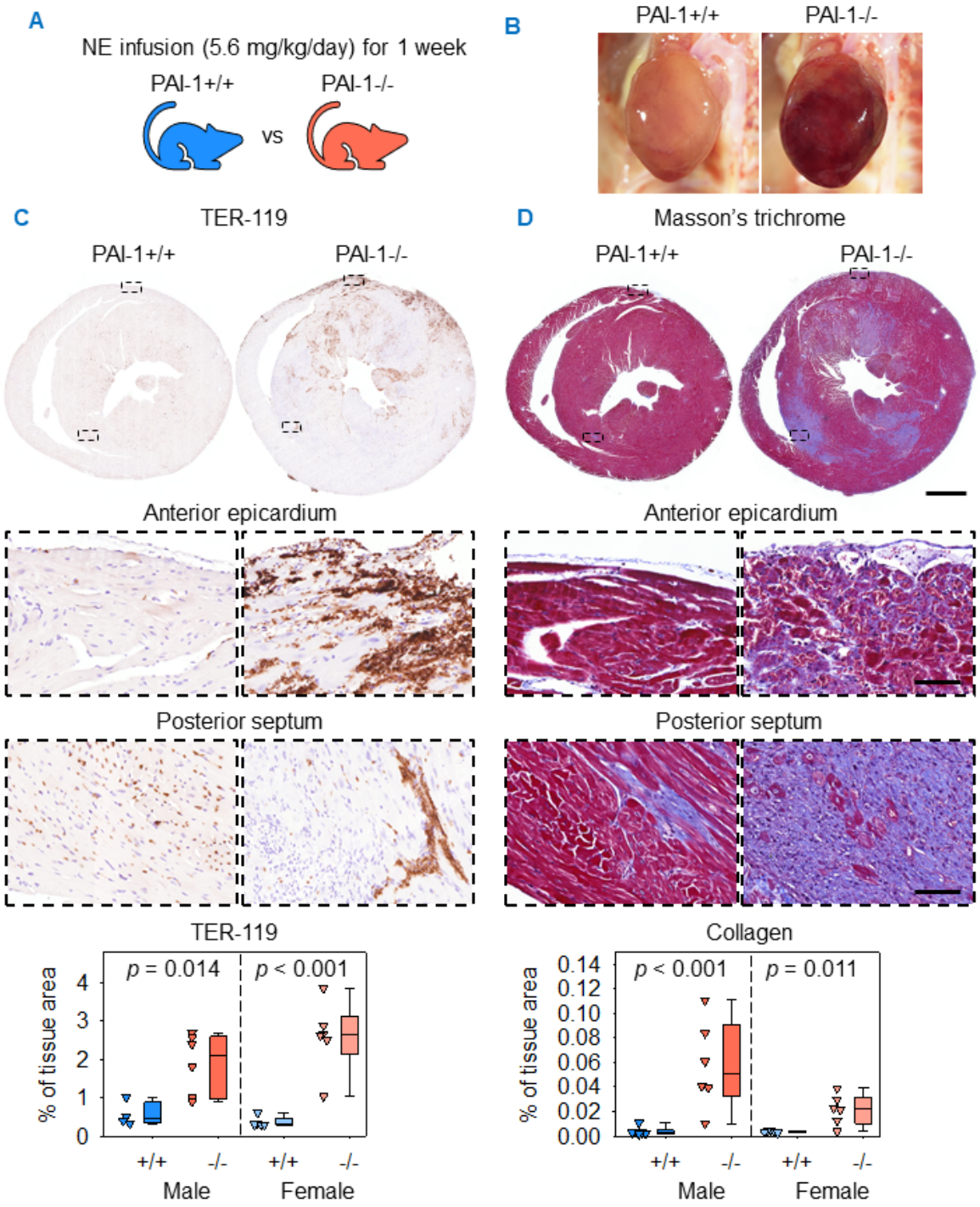


Figure 5. **PAI-1 deficiency augmented NE-induced cardiac fibrosis and promoted hemorrhage after 1 week of NE infusion**. (**A**) Male and female PAI-1+/+ and -/- littermates were infused with NE (5.6 mg/kg/day) for 1 week. (**B**) Representative *in situ* heart images. (**C**) Representative TER-119 immunohistochemistry and quantification of mid-ventricular hearts. Comparisons between genotypes were made by Student's *t* test for males and Student's *t* test after log transformation for females. (**D**) Representative Masson's trichrome staining and collagen quantification of mid-ventricular hearts. Comparisons between genotypes were made by Student's *t* test after log transformation for males and Student's *t* test for females. *n* = 5-6 mice/group. Representative images are from male mice. Scale bars = 1,000 μm and 100 μm for low and high-magnification images, respectively. Abbreviations: NE: norepinephrine, PAI-1: plasminogen activator inhibitor-1.

bioRxiv preprint doi: https://doi.org/10.1101/2025.11.19.689269; this version posted November 19, 2025. The copyright holder for this preprint (which was not certified by peer review) is the author/funder, who has granted bioRxiv a license to display the preprint in perpetuity. It is made available under aCC-BY 4.0 International license.

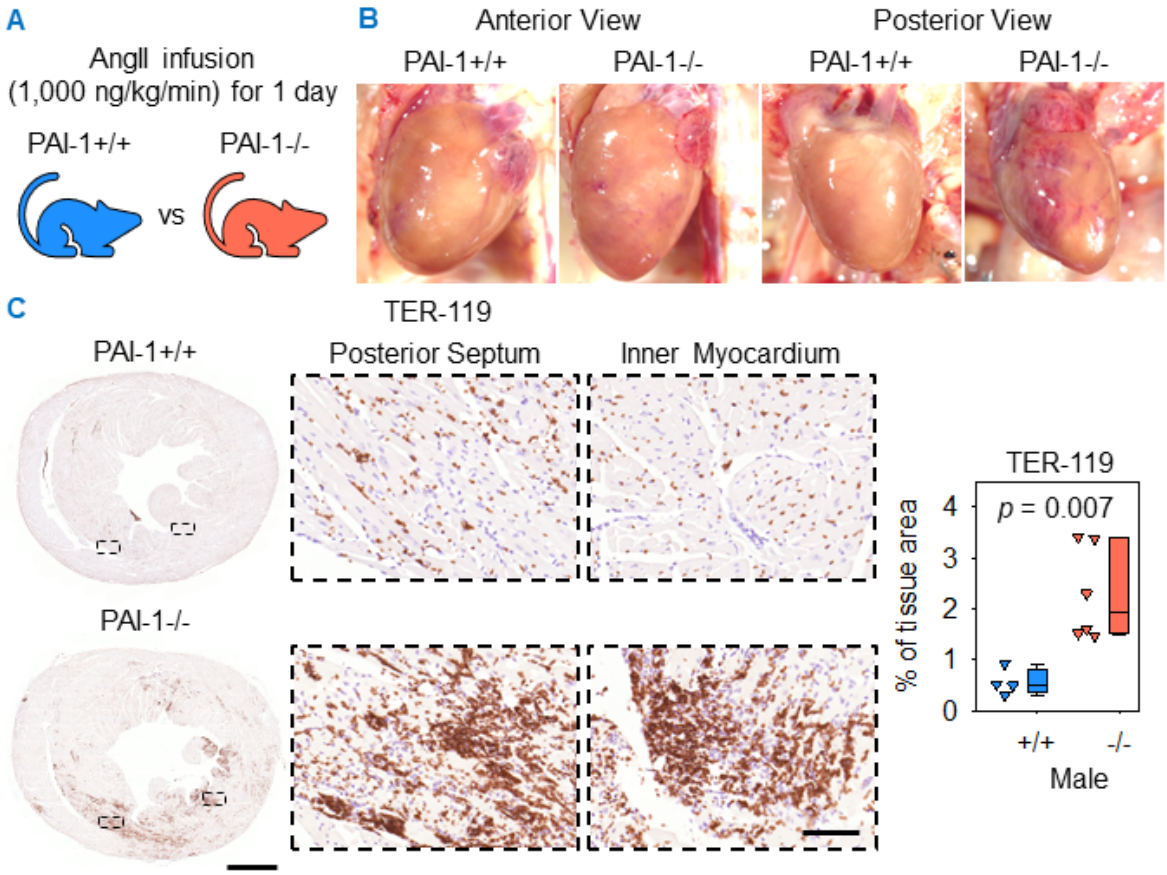


Figure 6. **PAI-1 deficiency induced cardiac hemorrhage after 1 day of AngII infusion.** (**A**) Male PAI-1+/+ and -/- littermates were infused with AngII (1,000 ng/kg/min) for 1 day. (**B**) Representative *in situ* heart images. (**C**) Representative TER-119 immunohistochemistry and color quantification in mid-ventricular heart sections. Comparison was made by Student's *t* test. *n* = 4-6 mice/group. Scale bars = 1,000 μm and 100 μm for low and high-magnification images, respectively. Abbreviations: AngII: angiotensin II, PAI-1: plasminogen activator inhibitor-1.

bioRxiv preprint doi: https://doi.org/10.1101/2025.11.19.689269; this version posted November 19, 2025. The copyright holder for this preprint (which was not certified by peer review) is the author/funder, who has granted bioRxiv a license to display the preprint in perpetuity. It is made available under aCC-BY 4.0 International license.

Cardiac Hemorrhage Precedes Hypertension-induced Fibrosis in Plasminogen Activator Inhibitor-1 Deficient Mice

Alex C. Pettey,[1,2] Sohei Ito,[2] Michael K. Franklin,[2] Deborah A. Howatt,[2] Jessica J. Moorleghen,[2] Bryana M. Levitan,[1] David B. Graf,[2] Valerie Z. Guzmán,[2] Nancy Zhang,[2] Hisashi Sawada,[1-3] Jeffrey E. Saffitz,[4] Hong S. Lu,[1-3] Alan Daugherty[1-3]

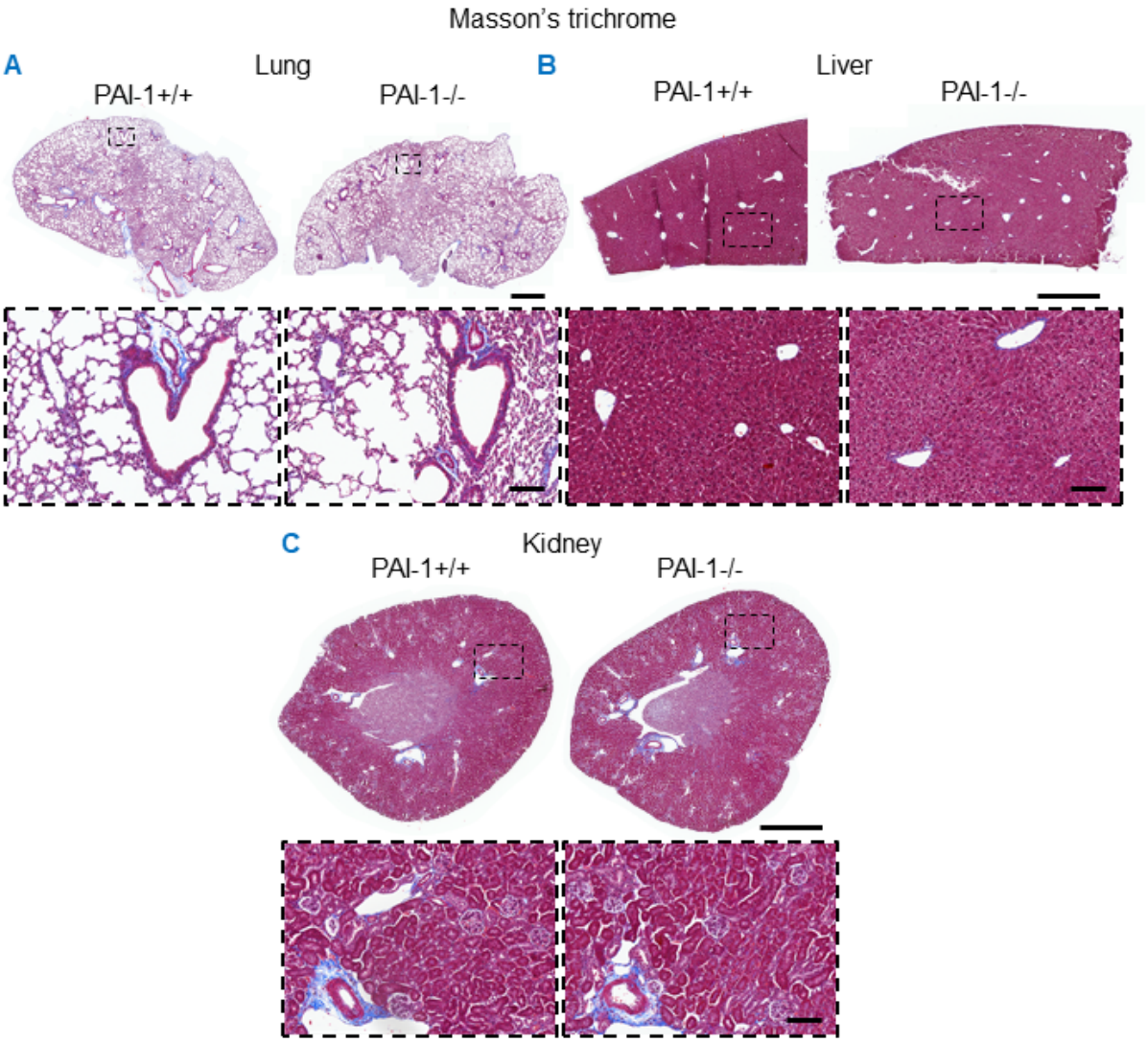
[1] Department of Physiology,
[2] Saha Cardiovascular Research Center
[3] Saha Aortic Center
University of Kentucky, Lexington, KY

[4] Department of Pathology, Beth Israel Deaconess Medical Center,
Harvard Medical School, Boston, MA

Corresponding authors:
Alan Daugherty
Saha CVRC, BBSRB, Room 243
University of Kentucky
741 S Limestone
Lexington KY 40356-0509
e-mail – alan.daugherty@uky.edu

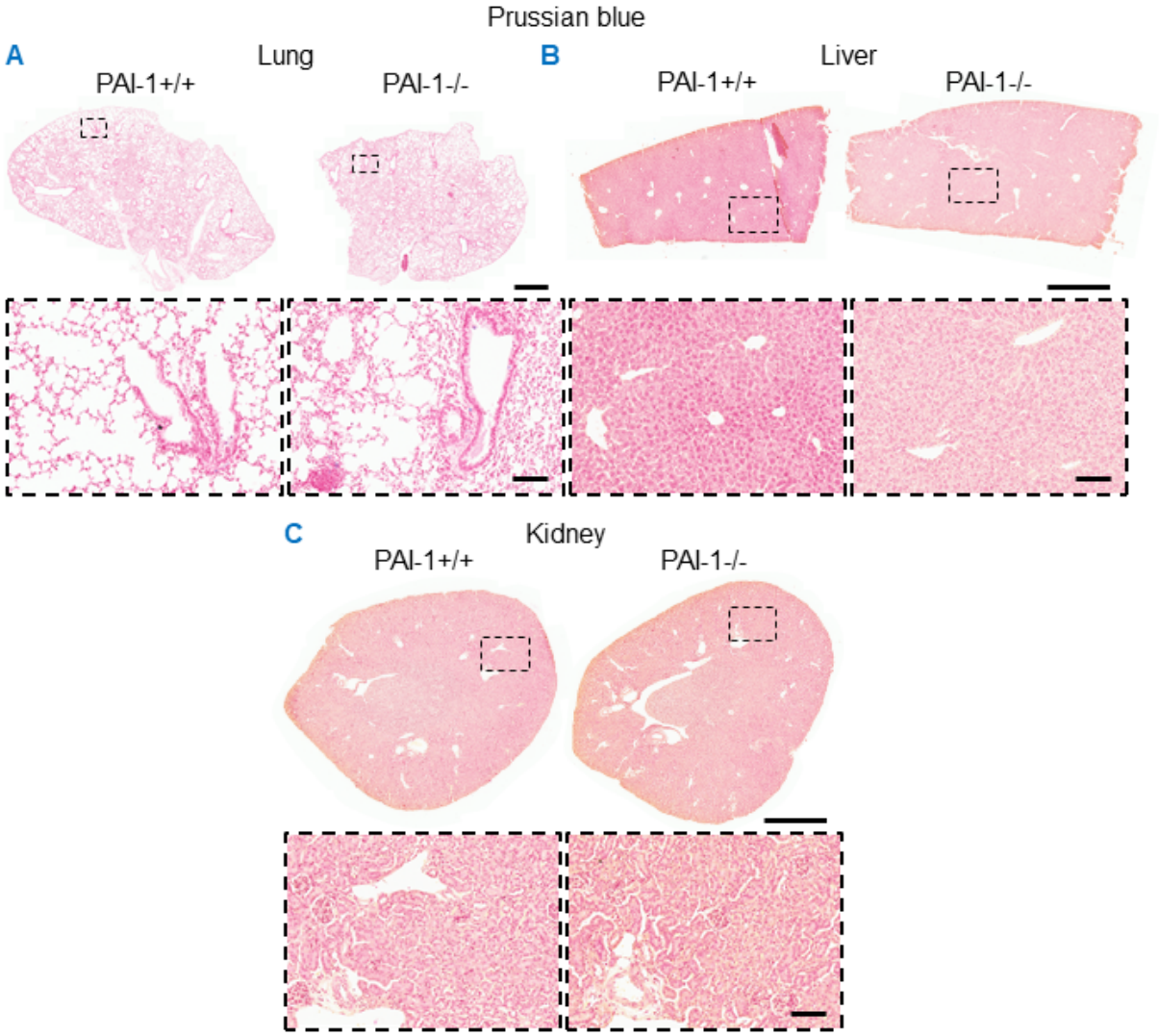
Hong S. Lu
Saha CVRC, BBSRB, Room 249
University of Kentucky
741 S Limestone
Lexington KY 40356-0509
e-mail – Hong.Lu@uky.edu

bioRxiv preprint doi: https://doi.org/10.1101/2025.11.19.689269; this version posted November 19, 2025. The copyright holder for this preprint (which was not certified by peer review) is the author/funder, who has granted bioRxiv a license to display the preprint in perpetuity. It is made available under aCC-BY 4.0 International license.



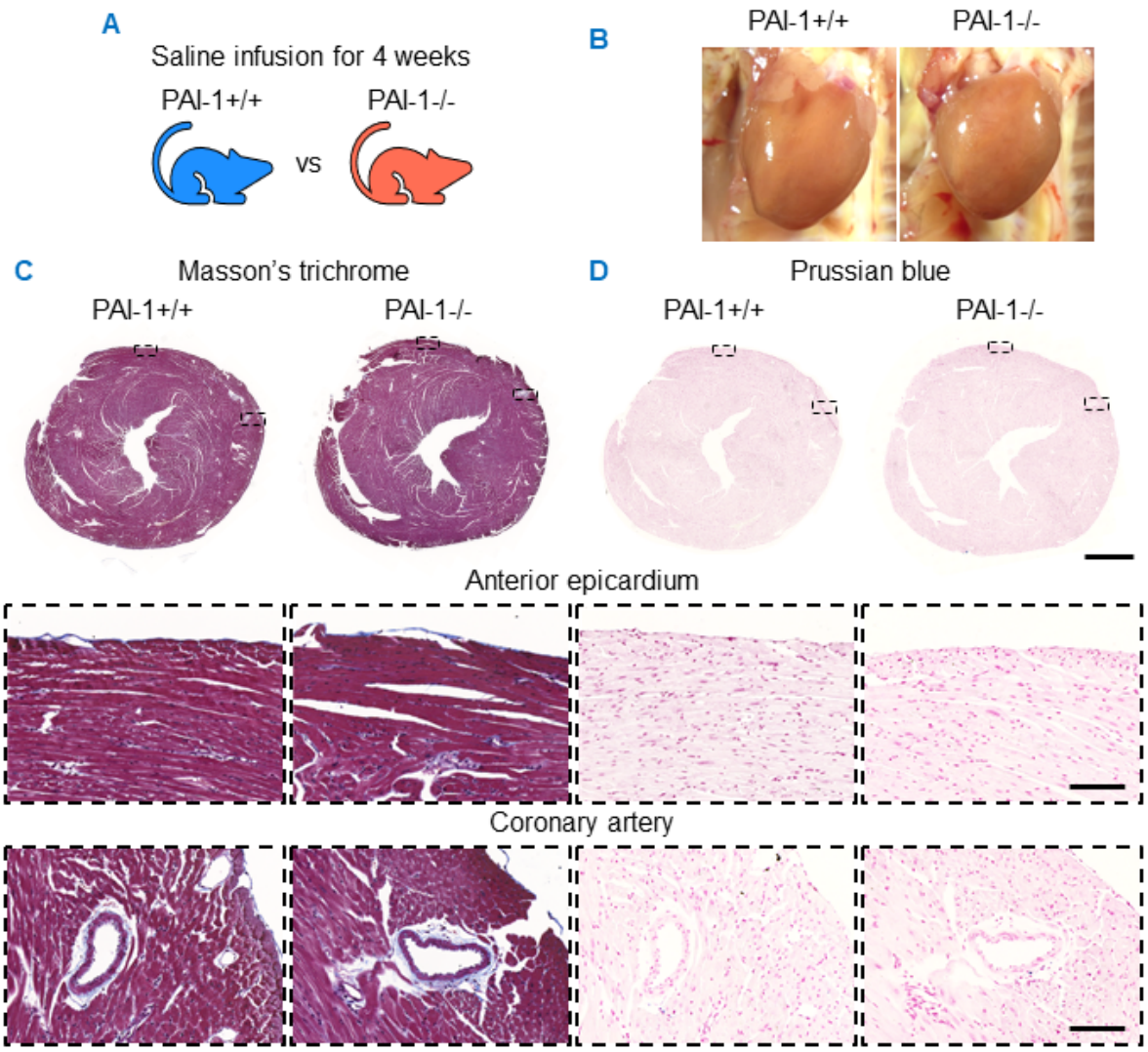
Supplemental Figure 1. PAI-1 deficiency did not overtly alert lung, liver, or kidney fibrosis. (**A-C**) Representative Masson's trichrome staining of left lung (**A**), left liver lobe (**B**), and left kidney sections (**C**) of mice infused with AngII (1,000 ng/kg/min) for 4 weeks. Representative images are from male mice. Scale bars = 1,000 μm and 100 μm for low and high-magnification images, respectively. Abbreviation: AngII: angiotensin II, PAI-1: plasminogen activator inhibitor-1.

bioRxiv preprint doi: https://doi.org/10.1101/2025.11.19.689269; this version posted November 19, 2025. The copyright holder for this preprint (which was not certified by peer review) is the author/funder, who has granted bioRxiv a license to display the preprint in perpetuity. It is made available under aCC-BY 4.0 International license.



Supplemental Figure 2. PAI-1 deficiency did not detectably alert lung, liver, or kidney ferric iron deposition. (**A-C**) Representative Prussian blue staining of left lung (**A**), left liver lobe (**B**), and left kidney sections (**C**) of mice infused with AngII (1,000 ng/kg/min) for 4 weeks. Representative images are from male mice. Scale bars = 1,000 μm and 100 μm for low and high-magnification images, respectively. Abbreviation: AngII: angiotensin II, PAI-1: plasminogen activator inhibitor-1.

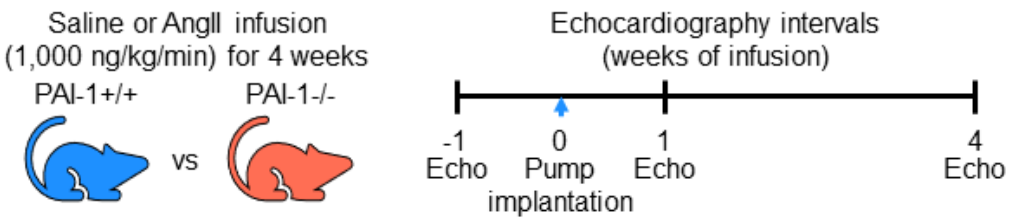
bioRxiv preprint doi: https://doi.org/10.1101/2025.11.19.689269; this version posted November 19, 2025. The copyright holder for this preprint (which was not certified by peer review) is the author/funder, who has granted bioRxiv a license to display the preprint in perpetuity. It is made available under aCC-BY 4.0 International license.



Supplemental Figure 3. **PAI-1 deficiency caused minimal cardiac pathology after 4 weeks of saline infusion.** (**A**) Male and female PAI-1+/+ and -/- littermates were infused with saline for 4 weeks. (**B**) Representative *in situ* heart images. (**C-D**) Representative Masson's trichrome (**C**) and Prussian blue staining (**D**) of hearts. Representative images are from male mice. Scale bars = 1,000 μm and 100 μm for low and high-magnification images, respectively. Abbreviation: PAI-1: plasminogen activator inhibitor-1.

bioRxiv preprint doi: https://doi.org/10.1101/2025.11.19.689269; this version posted November 19, 2025. The copyright holder for this preprint (which was not certified by peer review) is the author/funder, who has granted bioRxiv a license to display the preprint in perpetuity. It is made available under aCC-BY 4.0 International license.

A



B

Males

Group	Time (weeks)	LVID;d (mm)	LV mass (mg)	LVAW;d (mm)	LVPW;d (mm)	EF (%)	GLS (%)	GCS (%)
PAI-1+/+ saline	-1	3.6 ± 0.2	105 ± 7	0.9 ± 0.05	0.8 ± 0.02	59 ± 3	-21 ± 1	-19 ± 1
	1	4 ± 0.1	117 ± 4	0.9 ± 0.03	0.7 ± 0.03	56 ± 1	-20 ± 2	-22 ± 1
	4	4.1 ± 0.1	130 ± 5	0.9 ± 0.02	0.8 ± 0.04	59 ± 5	-16 ± 1	-22 ± 3
PAI-1-/- saline	-1	3.9 ± 0.2	115 ± 11	0.9 ± 0.07	0.7 ± 0.05	58 ± 7	-20 ± 2	-22 ± 3
	1	3.9 ± 0.1	120 ± 6	0.9 ± 0.03	0.8 ± 0.08	66 ± 2	-18 ± 2	-22 ± 2
	4	3.9 ± 0.1	123 ± 6	0.9 ± 0.05	0.8 ± 0.03	60 ± 3	-16 ± 2	-21 ± 2
PAI-1+/+ AngII	-1	3.8 ± 0.1	108 ± 7	0.9 ± 0.08	0.7 ± 0.03	63 ± 4	-16 ± 1	-22 ± 2
	1	3.9 ± 0.2	149 ± 7	1.1 ± 0.09	0.9 ± 0.03	53 ± 2	-12 ± 2	-16 ± 2
	4	4.1 ± 0.1	148 ± 10	1.1 ± 0.08	0.8 ± 0.06	48 ± 5	-12 ± 2	-17 ± 3
PAI-1-/- AngII	-1	4 ± 0.2	117 ± 4	0.9 ± 0.05	0.7 ± 0.03	57 ± 3	-18 ± 1	-20 ± 2
	1	3.6 ± 0.2	199 ± 25	1.4 ± 0.19	1.1 ± 0.08	55 ± 6	-8 ± 1	-17 ± 2
	4	4.4 ± 0.3	171 ± 20	1.1 ± 0.06	0.8 ± 0.04	48 ± 4	-10 ± 2	-15 ± 1
p values	Group	> 0.99	0.003	0.056	0.009	0.18	< 0.001	0.04
	Time	0.026	< 0.001	0.002	< 0.001	0.11	< 0.001	0.5
	Interaction	0.24	0.071	0.088	0.002	0.25	0.23	0.28

C

Females

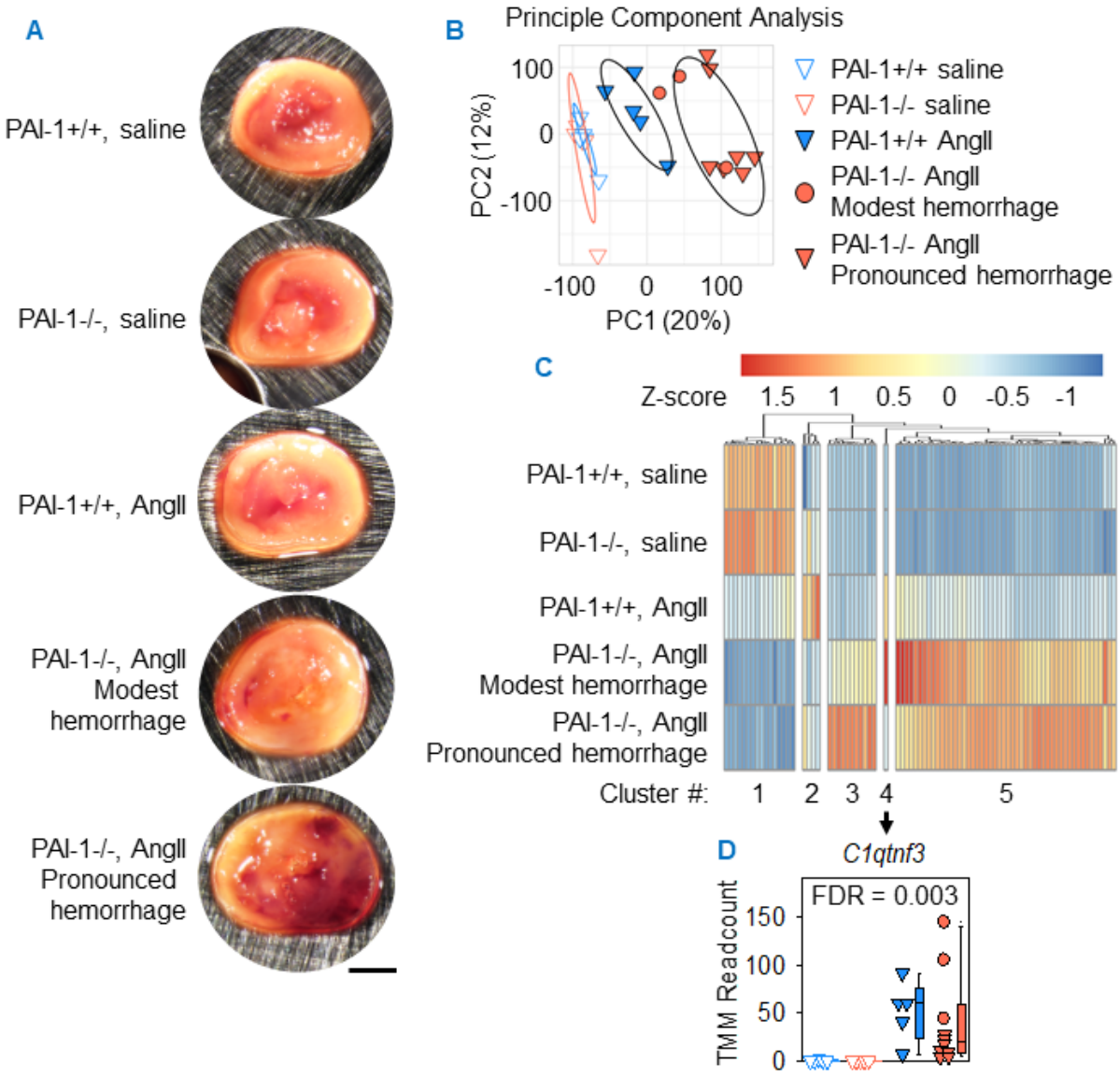
Group	Time (weeks)	LVID;d (mm)	LV mass (mg)	LVAW;d (mm)	LVPW;d (mm)	EF (%)	GLS (%)	GCS (%)
PAI-1+/+ saline	-1	3.6 ± 0.2	83 ± 5	0.8 ± 0.05	0.6 ± 0.05	55 ± 4	-16 ± 2	-23 ± 3
	1	3.7 ± 0.2	97 ± 8	0.8 ± 0.03	0.7 ± 0.04	65 ± 5	-19 ± 2	-23 ± 0
	4	3.6 ± 0.1	106 ± 8	0.9 ± 0.04	0.8 ± 0.04	66 ± 2	-19 ± 2	-23 ± 1
PAI-1-/- saline	-1	3.7 ± 0.1	92 ± 6	0.7 ± 0.02	0.7 ± 0.03	54 ± 2	-16 ± 1	-18 ± 2
	1	3.8 ± 0.1	103 ± 6	0.9 ± 0.05	0.7 ± 0.04	56 ± 2	-16 ± 1	-19 ± 1
	4	3.5 ± 0.1	107 ± 5	0.9 ± 0.05	0.8 ± 0.04	66 ± 3	-18 ± 2	-25 ± 3
PAI-1+/+ AngII	-1	3.5 ± 0.1	86 ± 5	0.8 ± 0.04	0.7 ± 0.02	59 ± 3	-17 ± 1	-23 ± 1
	1	3.7 ± 0.1	114 ± 6	0.9 ± 0.05	0.8 ± 0.03	55 ± 2	-16 ± 2	-19 ± 3
	4	3.7 ± 0.1	120 ± 9	1 ± 0.06	0.8 ± 0.04	58 ± 2	-14 ± 2	-18 ± 2
PAI-1-/- AngII	-1	3.4 ± 0.1	77 ± 4	0.7 ± 0.02	0.7 ± 0.03	60 ± 3	-15 ± 1	-18 ± 2
	1	3.3 ± 0.1	136 ± 19	1.2 ± 0.15	1 ± 0.09	59 ± 2	-11 ± 1	-17 ± 1
	4	3.2 ± 0.04	108 ± 5	1 ± 0.07	0.9 ± 0.04	68 ± 4	-12 ± 1	-21 ± 2
p values	Group	0.010	0.61	0.25	0.070	0.17	0.010	0.10
	Time	0.18	< 0.001	< 0.001	< 0.001	0.007	0.62	0.36
	Interaction	0.46	0.16	0.25	0.010	0.25	0.31	0.23

Supplemental Figure 4. PAI-1 deficiency did not alter systolic function within 4 weeks of AngII infusion. (**A**) Male PAI-1+/+ and -/- littermates were infused with saline or AngII (1,000 ng/kg/min) for 4 weeks. Echocardiography was performed 1 week prior to

bioRxiv preprint doi: https://doi.org/10.1101/2025.11.19.689269; this version posted November 19, 2025. The copyright holder for this preprint (which was not certified by peer review) is the author/funder, who has granted bioRxiv a license to display the preprint in perpetuity. It is made available under aCC-BY 4.0 International license.

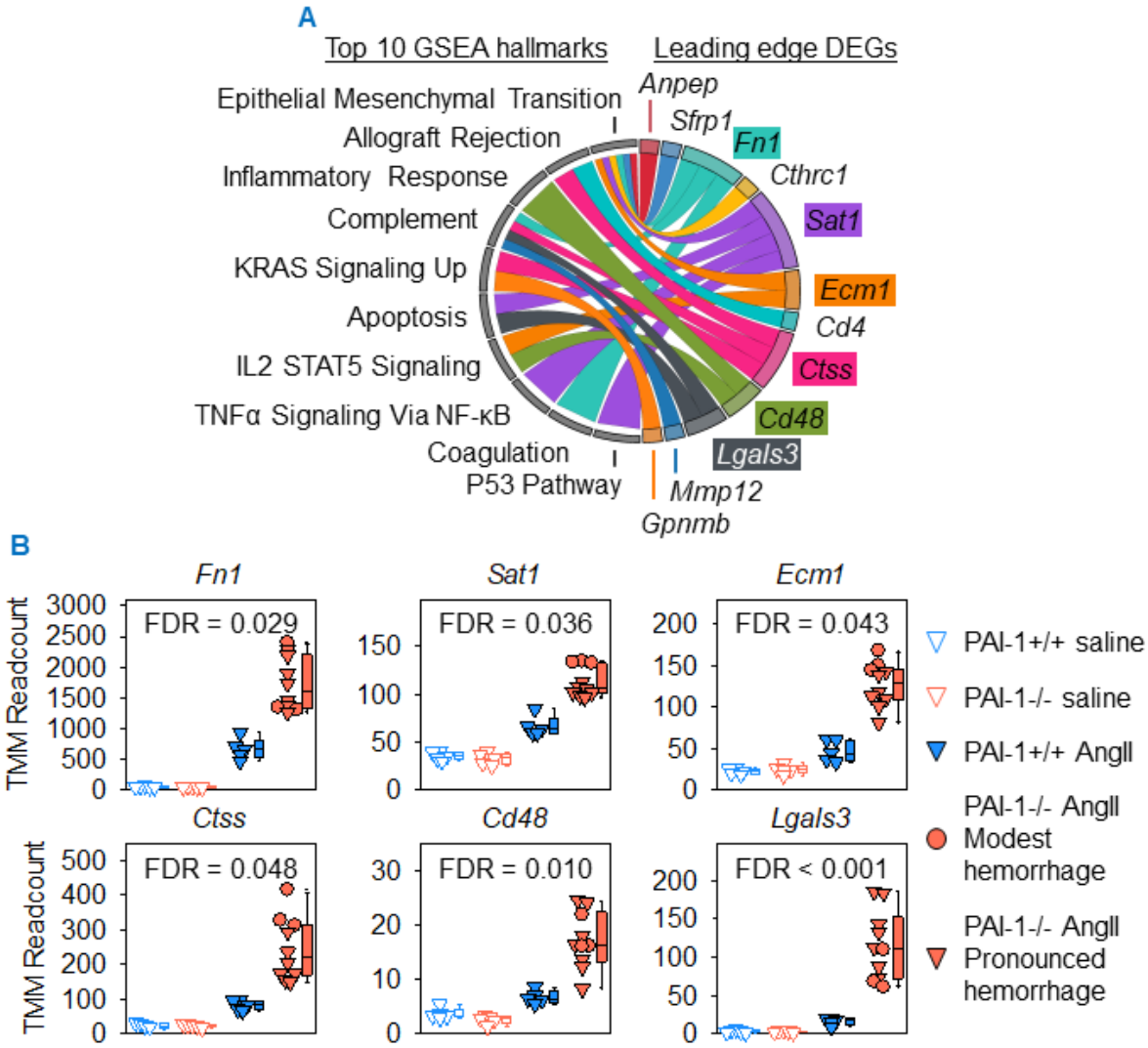
pump implant (-1) and at 1 and 4 weeks of infusion. (**B-C**) Summary tables of echocardiography parameters in male (**B**) and female mice (**C**). The following transformations were applied prior to analysis: for males: LVPW;d, EF, GLS, and GCS: no transformation; LVID;d: inverse; LV mass and LVAW;d: Box–Cox; for females: LVID;d, GLS, and GCS: no transformation; LV mass: inverse; LVAW;d, LVPW;d, and EF: Box–Cox. Comparisons between groups were made by two-way repeated measures ANOVA. (**B**) n = 7 – 8 mice/group. (**C**) n = 4 – 10 mice/group. Abbreviations: AngII: angiotensin II, PAI-1: plasminogen activator inhibitor-1, Echo: echocardiography, LVID;d: left ventricular internal diameter; diastole, LV: left ventricle, LVAW;d: left ventricle anterior wall; diastole, LVPW;d left ventricle posterior wall; diastole, EF: ejection fraction, GLS: global longitudinal strain, GCS: global circumferential strain.

bioRxiv preprint doi: https://doi.org/10.1101/2025.11.19.689269; this version posted November 19, 2025. The copyright holder for this preprint (which was not certified by peer review) is the author/funder, who has granted bioRxiv a license to display the preprint in perpetuity. It is made available under aCC-BY 4.0 International license.



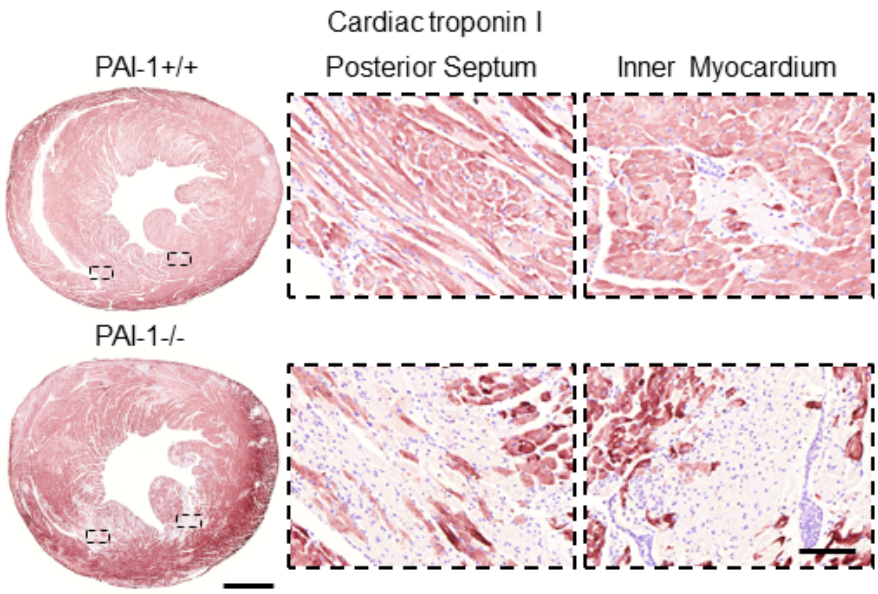
Supplemental Figure 5. PAI-1 deficiency augmented AngII-induced cardiac transcriptomic alterations after 1 week of infusion. Male PAI-1+/+ and -/- littermates were infused with saline or AngII (1,000 ng/kg/min) for 1 week. (**A**) Representative images of mid-ventricular heart sections used for bulk RNA-sequencing. Scale bar = 1,000 μm. (**B**) Principal component analysis of heart transcriptomes. Ellipses represent 75% confidence intervals. (**C**) Z-scored heatmap of all genes differentially expressed by interaction analysis of genotype and infusion controlling for the presence of pronounced hemorrhage. (**D**) Normalized read count expression of *C1qtnf3*, the sole transcript in cluster #4. Legend applies to (**B**) and (**D**). *n* = 5-10 mice/group. Abbreviations: PAI-1: plasminogen activator inhibitor-1, AngII: angiotensin II, PC: principal component, TMM: trimmed mean of M-values, FDR: false discovery rate.

bioRxiv preprint doi: https://doi.org/10.1101/2025.11.19.689269; this version posted November 19, 2025. The copyright holder for this preprint (which was not certified by peer review) is the author/funder, who has granted bioRxiv a license to display the preprint in perpetuity. It is made available under aCC-BY 4.0 International license.



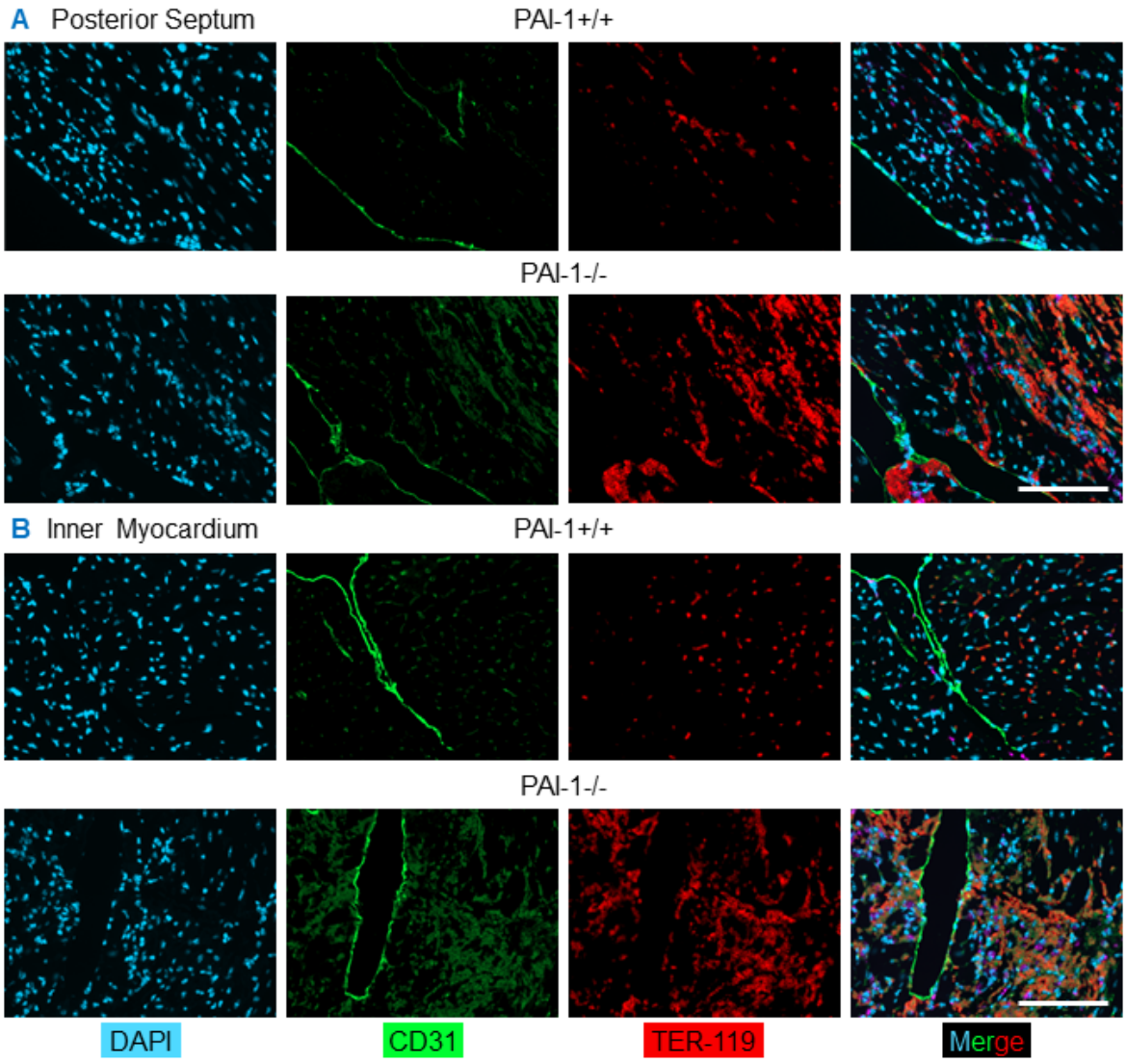
Supplemental Figure 6. PAI-1 deficiency increased transcripts related to proteolysis and fibrosis independently of hemorrhage presence after 1 week of AngII infusion. (**A**) Chord graph representing the top 10 GSEA hallmark gene sets and interaction DEGs present within the leading edge of corresponding Hallmark gene sets. (**B**) Normalized read count expression of interaction DEGs present in the leading edge of at least two top-10 GSEA Hallmark gene sets. *n* = 5-10 mice/group. Abbreviations: AngII: angiotensin II, PAI-1: plasminogen activator inhibitor-1, GSEA: gene set enrichment analysis, DEG: differentially expressed gene, TMM: trimmed mean of M-values, FDR: false discovery rate.

bioRxiv preprint doi: https://doi.org/10.1101/2025.11.19.689269; this version posted November 19, 2025. The copyright holder for this preprint (which was not certified by peer review) is the author/funder, who has granted bioRxiv a license to display the preprint in perpetuity. It is made available under aCC-BY 4.0 International license.



Supplemental Figure 7. PAI-1 deficiency induced cardiomyocyte injury after 1 day of AngII infusion. Male PAI-1+/+ and -/- littermates were infused with AngII (1,000 ng/kg/min) for 1 day. Representative cardiac troponin I immuno-histochemistry in mid-ventricular heart sections. Scale bars = 1,000 μm and 100 μm for low and high-magnification images, respectively. Abbreviations: AngII: angiotensin II, PAI-1: plasminogen activator inhibitor-1.

bioRxiv preprint doi: https://doi.org/10.1101/2025.11.19.689269; this version posted November 19, 2025. The copyright holder for this preprint (which was not certified by peer review) is the author/funder, who has granted bioRxiv a license to display the preprint in perpetuity. It is made available under aCC-BY 4.0 International license.



Supplemental Figure 8. PAI-1 deficiency induced erythrocyte extravasation after 1 day of AngII infusion. Male PAI-1+/+ and -/- littermates were infused with AngII (1,000 ng/kg/min) for 1 day. (**A-B**) Representative co-immunofluorescent staining for DAPI, CD31, and TER-119 in (**A**) the posterior septum and (**B**) the inner myocardium of mid-ventricular heart sections. Scale bars = 100 μm. Abbreviations: AngII: angiotensin II, PAI-1: plasminogen activator inhibitor-1, DAPI: 4',6-diamidino-2-phenylindole.

bioRxiv preprint doi: https://doi.org/10.1101/2025.11.19.689269; this version posted November 19, 2025. The copyright holder for this preprint (which was not certified by peer review) is the author/funder, who has granted bioRxiv a license to display the preprint in perpetuity. It is made available under aCC-BY 4.0 International license.

MAJOR RESOURCES TABLES

Primer sequences for genotyping of PAI-1

Gene (Forward / Reverse)	Vendor or Source	Primer Sequence (5'-3')
PAI-1 (forward)	Integrated DNA Technologies	CTGGGCAGTAACCCAAGAGA
PAI-1 (wild type reverse)	Integrated DNA Technologies	GTCGGTCGTCTAGACCCTTG
PAI-1 (mutant reverse)	Integrated DNA Technologies	TGGATGTGGAATGTGTGCGAG

Blocking reagents for immunostaining

Reagent	Vendor	Catalog #
Normal goat serum	Vector laboratories	30024
Normal horse serum	Vector laboratories	30022

Primary antibodies for immunostaining

Antibody	Vendor	Catalog #	Working concentration
Rat anti-TER-119	Thermo Scientific	15-5921-82	0.3 µg/mL
Rabbit anti-cardiac troponin I	abcam	ab47003	1.0 µg/mL
Goat anti-CD31	R&D Systems	AF3628	17.8 µg/mL

Secondary antibodies for immunostaining

Antibody	Vendor	Catalog #	Working concentration
ImmPRESS HRP goat anti-rat IgG	Vector Laboratories	30033	as supplied
ImmPRESS HRP goat anti-rabbit IgG	Vector Laboratories	30125	as supplied
Alexa-647 donkey anti-rat IgG	abcam	ab150155	2.0 µg/mL
Alexa-488 donkey anti-goat IgG	abcam	ab150129	2.0 µg/mL

RGB thresholds for histology and immunostaining quantification

Stain	Feature	Thresholds		
		Red	Green	Blue
Masson's trichrome	Collagen	0–180	0–190	200–255
	Background	220–255	200–255	215–255
Prussian blue	Ferric iron	30–150	40–160	70–240
	Background	250–255	250–255	250–255
TER-119	Erythrocytes	85–200	40–140	10–110
	Background	250–255	250–255	250–255

Figure 1

Inclusion Criteria	Exclusion Criteria
• Male and female • 8-14 weeks of age • PAI-1+/+ and PAI-1-/-	• Death prior to endpoint • Euthanasia prior to endpoint for humane reasons as based on IACUC regulations • Heterozygous genotype determined at endpoint verification

bioRxiv preprint doi: https://doi.org/10.1101/2025.11.19.689269; this version posted November 19, 2025. The copyright holder for this preprint (which was not certified by peer review) is the author/funder, who has granted bioRxiv a license to display the preprint in perpetuity. It is made available under aCC-BY 4.0 International license.

	• Plasma renin concentration (PRC) > 10 ng/ml/hour at endpoint				
Groups	**Sex**	**Age (weeks)**	**Number (prior to experiment)**	**Number (termination)**	**Exclusions**
PAI-1+/+, AngII for 4 weeks	M	8-14	14	12	(*n* = 2) death prior to endpoint
PAI-1-/-, AngII for 4 weeks	M	8-14	10	9	(*n* = 1) PRC > 10 ng/ml/hour at endpoint
PAI-1+/+, AngII for 4 weeks	F	8-14	11	11	none
PAI-1-/-, AngII for 4 weeks	F	8-14	22	16	(*n* = 2) heterozygous genotype at endpoint; (*n* = 4) PRC > 10 ng/ml/hour at endpoint

Figure 2

Inclusion/Exclusion Criteria					
Inclusion and exclusion criteria are identical to those in Figure 1, with the following additional inclusion criteria: • Random selection within groups when no gross cardiac pathology is present • Selection representative of the full range of observed gross cardiac pathology, when present					
Groups	**Sex**	**Age (weeks)**	**Number (termination)**	**Number (histology)**	**Inclusion**
PAI-1+/+, AngII for 4 weeks	M	8-14	12	8	Random selection
PAI-1-/-, AngII for 4 weeks	M	8-14	9	7	Full range of gross pathology
PAI-1+/+, AngII for 4 weeks	F	8-14	11	8	Random selection
PAI-1-/-, AngII for 4 weeks	F	8-14	16	9	Full range of gross pathology

Refer to Figure 1 table for the number of mice prior to experiment initiation and for exclusions.

bioRxiv preprint doi: https://doi.org/10.1101/2025.11.19.689269; this version posted November 19, 2025. The copyright holder for this preprint (which was not certified by peer review) is the author/funder, who has granted bioRxiv a license to display the preprint in perpetuity. It is made available under aCC-BY 4.0 International license.

Figure 3

Inclusion Criteria	Exclusion Criteria
• Male and female • 10-12 weeks of age • PAI-1+/+ and PAI-1-/- • Random selection within groups when no gross cardiac pathology is present • Selection representative of the full range of observed gross cardiac pathology, when present	• Death prior to endpoint • Euthanasia prior to endpoint for humane reasons as based on IACUC regulations • Heterozygous genotype determined at endpoint verification

Groups	Sex	Age (weeks)	Number (prior to experiment)	Number (histology)	Inclusion / Exclusion
PAI-1+/+, NE for 4 weeks	M	11-12	7	5	Exclusion: (*n* = 1) heterozygous genotype at endpoint; (*n* = 1) death prior to endpoint Inclusion: random selection
PAI-1-/-, NE for 4 weeks	M	11-12	10	8	Exclusion: none Inclusion: full range of gross pathology
PAI-1+/+, NE for 4 weeks	F	11-12	9	6	Exclusion: none Inclusion: random selection
PAI-1-/-, NE for 4 weeks	F	11-12	10	5	Exclusion: none Inclusion: full range of gross pathology

bioRxiv preprint doi: https://doi.org/10.1101/2025.11.19.689269; this version posted November 19, 2025. The copyright holder for this preprint (which was not certified by peer review) is the author/funder, who has granted bioRxiv a license to display the preprint in perpetuity. It is made available under aCC-BY 4.0 International license.

Figure 4

Inclusion Criteria	Exclusion Criteria
• Male and female • 10-12 weeks of age • PAI-1+/+ and PAI-1-/- • Random selection within groups when no gross cardiac pathology is present • Selection representative of the full range of observed gross cardiac pathology, when present	• Death prior to endpoint • Euthanasia prior to endpoint for humane reasons as based on IACUC regulations • Heterozygous genotype determined at endpoint verification • Plasma renin concentration (PRC) > 10 ng/ml/hour at endpoint

Groups	Sex	Age (weeks)	Number (prior to experiment)	Number (histology)	Inclusion / Exclusion
PAI-1+/+, AngII for 1 week	M	11-12	12	6	Exclusion: (*n* = 2) heterozygous genotype at endpoint Inclusion: random selection
PAI-1-/-, AngII for 1 week	M	11-12	15	5	Exclusion: (*n* = 3) heterozygous genotype at endpoint; (*n* = 3) death prior to endpoint; (*n* = 3) PRC > 10 ng/ml/hour at endpoint Inclusion: full range of gross pathology
PAI-1+/+, AngII for 1 week	F	11-12	18	7	Exclusion: (*n* = 2) heterozygous genotype at endpoint Inclusion: random selection
PAI-1-/-, AngII for 1 week	F	11-12	16	6	Exclusion: (*n* = 1) heterozygous genotype at endpoint; (*n* = 1) death prior to endpoint Inclusion: full range of gross pathology

bioRxiv preprint doi: https://doi.org/10.1101/2025.11.19.689269; this version posted November 19, 2025. The copyright holder for this preprint (which was not certified by peer review) is the author/funder, who has granted bioRxiv a license to display the preprint in perpetuity. It is made available under aCC-BY 4.0 International license.

Figure 5

Inclusion Criteria	Exclusion Criteria
• Male and female • 10-12 weeks of age • PAI-1+/+ and PAI-1-/- • Random selection within groups when no gross cardiac pathology is present • Selection representative of the full range of observed gross cardiac pathology, when present	• Death prior to endpoint • Euthanasia prior to endpoint for humane reasons as based on IACUC regulations • Heterozygous genotype determined at endpoint verification

Groups	Sex	Age (weeks)	Number (prior to experiment)	Number (histology)	Inclusion / Exclusion
PAI-1+/+, NE for 1 week	M	11-12	10	6	Exclusion: (*n* = 1) heterozygous genotype at endpoint Inclusion: random selection
PAI-1-/-, NE for 1 week	M	11-12	9	6	Exclusion: none Inclusion: full range of gross pathology
PAI-1+/+, NE for 1 week	F	11-12	5	5	Exclusion: none Inclusion: all
PAI-1-/-, NE for 1 week	F	11-12	10	6	Exclusion: none Inclusion: full range of gross pathology

Figure 6

Inclusion Criteria	Exclusion Criteria
• Male and female • 10-12 weeks of age • PAI-1+/+ and PAI-1-/-	• Death prior to endpoint • Euthanasia prior to endpoint for humane reasons as based on IACUC regulations • Heterozygous genotype determined at endpoint verification

Groups	Sex	Age (weeks)	Number (prior to experiment)	Number (termination)	Exclusions
PAI-1+/+, AngII for 1 day	M	9-12	6	4	(*n* = 2) heterozygous genotype at endpoint
PAI-1-/-, AngII for 1 day	M	9-12	7	6	(*n* = 1) heterozygous genotype at endpoint

bioRxiv preprint doi: https://doi.org/10.1101/2025.11.19.689269; this version posted November 19, 2025. The copyright holder for this preprint (which was not certified by peer review) is the author/funder, who has granted bioRxiv a license to display the preprint in perpetuity. It is made available under aCC-BY 4.0 International license.

Supplemental Figure 4

Inclusion Criteria	Exclusion Criteria
• Male and female • 10-12 weeks of age • PAI-1+/+ and PAI-1-/-	• Death prior to endpoint • Euthanasia prior to endpoint for humane reasons as based on IACUC regulations • Heterozygous genotype determined at endpoint verification

Groups	Sex	Age (weeks)	Number (prior to experiment)	Number (termination)	Exclusions
PAI-1+/+, saline for 4 weeks	M	10-12	8	7	(*n* = 1) heterozygous genotype at endpoint
PAI-1-/-, saline for 4 weeks	M	10-12	9	8	(*n* = 1) death prior to endpoint
PAI-1+/+, AngII for 4 weeks	M	10-12	10	8	(*n* = 1) heterozygous genotype at endpoint; (*n* = 1) death prior to endpoint
PAI-1-/-, AngII for 4 weeks	M	10-12	11	7	(*n* = 1) heterozygous genotype at endpoint; (*n* = 3) death prior to endpoint
PAI-1+/+, saline for 4 weeks	F	10-12	6	4	(*n* = 2) heterozygous genotype at endpoint
PAI-1-/-, saline for 4 weeks	F	10-12	11	10	(*n* = 1) heterozygous genotype at endpoint
PAI-1+/+, AngII for 4 weeks	F	10-12	7	6	(*n* = 1) death prior to endpoint
PAI-1-/-, AngII for 4 weeks	F	10-12	11	9	(*n* = 1) heterozygous genotype at endpoint; (*n* = 1) death prior to endpoint

bioRxiv preprint doi: https://doi.org/10.1101/2025.11.19.689269; this version posted November 19, 2025. The copyright holder for this preprint (which was not certified by peer review) is the author/funder, who has granted bioRxiv a license to display the preprint in perpetuity. It is made available under aCC-BY 4.0 International license.

Supplemental Figure 5-6

Inclusion Criteria	Exclusion Criteria
• Male and female • 10-12 weeks of age • PAI-1+/+ and PAI-1-/- • Within AngII-infused PAI-1-/-: visible hemorrhage < 5% and ≥ 5% of tissue area = modest and pronounced hemorrhage, respectively	• Death prior to endpoint • Euthanasia prior to endpoint for humane reasons as based on IACUC regulations • Heterozygous genotype determined at endpoint verification • RNA integrity number (RIN) < 6.8

Groups	Sex	Age (weeks)	Number (prior to experiment)	Number (termination)	Exclusion
PAI-1+/+, saline for 1 week	M	8-12	5	5	none
PAI-1-/-, saline for 1 week	M	8-12	6	5	(*n* = 1) RIN < 6.8
PAI-1+/+, AngII for 1 week	M	8-12	5	5	none
PAI-1-/-, AngII for 1 week	M	8-12	11	10	(*n* = 1) death prior to endpoint

bioRxiv preprint doi: https://doi.org/10.1101/2025.11.19.689269; this version posted November 19, 2025. The copyright holder for this preprint (which was not certified by peer review) is the author/funder, who has granted bioRxiv a license to display the preprint in perpetuity. It is made available under aCC-BY 4.0 International license.

ARRIVE Guidelines Checklists

Item	Application
Ethics	Approved by the University of Kentucky IACUC (2018-2967)
Sex	For 1 and 4-week infusion pathological studies, both male and female animals were examined, and similar findings were reported for both sexes. Since no apparent sexual dimorphism was observed in AngII or NE-induced pathology, only male mice were examined for the 1-week bulk RNA sequencing and 1-day AngII infusion studies.
Inclusion / Exclusion criteria	Criteria were determined *a priori* and are listed for individual experiments within the Major Resources Tables.
Sample size	Described in each figure legend.
Sample size calculation	Figure 1: *n* = 9/group were calculated to detect a 0.3 ± 0.2 mm (mean ± SD) difference in aortic diameter (*t* test, α error = 0.05 and power = 0.8). Supplemental Figure 5: *n* = 9/group were calculated to detect a 20 ± 10% (mean ± SD) difference in ejection fraction (ANOVA, α error = 0.05 and power = 0.8). Supplemental Figure 6: *n* = 7/group were calculated to detect a 6 ± 3.6% (mean ± SD) difference in cardiac collagen staining (*t* test, α error = 0.05 and power = 0.8). Sample size calculations were not performed for the remaining figures.
Endpoint	Figure 1: ascending aortic diameters. Figures 2-3: cardiac collagen and ferric iron. Figures 4-5: cardiac collagen and TER-119. Figure 6: cardiac TER-119. Supplemental Figure 5: ejection fraction.
Randomization	Mice were randomly assigned to cages at weaning by sex. After stratifying by age, mice were randomly assigned to study groups. Mice were terminated without predetermined order.
Blinding	Genotyping, measurement of ultrasound images and *in situ* aortas, and quantification of histology were performed by an investigator blinded to the study group information. RNA sequencing library generation was performed by a 3rd party blinded to the study group information. All experimental data were verified by an independent investigator blinded to the study group information.
Statistical analysis	SigmaPlot (v15.0, SYSTAT Software Inc.) or R (v4.5.1).
Statistical method	Described in each figure legend.
Data availability	RNA sequencing data (raw FASTQ and aligned data) will be made publicly available at the Gene Expression Omnibus (GEO) repository. Numerical data that support the findings of this study are provided in the Supporting Data Values file. The data that support the findings of this study are also available from the corresponding authors on reasonable request.